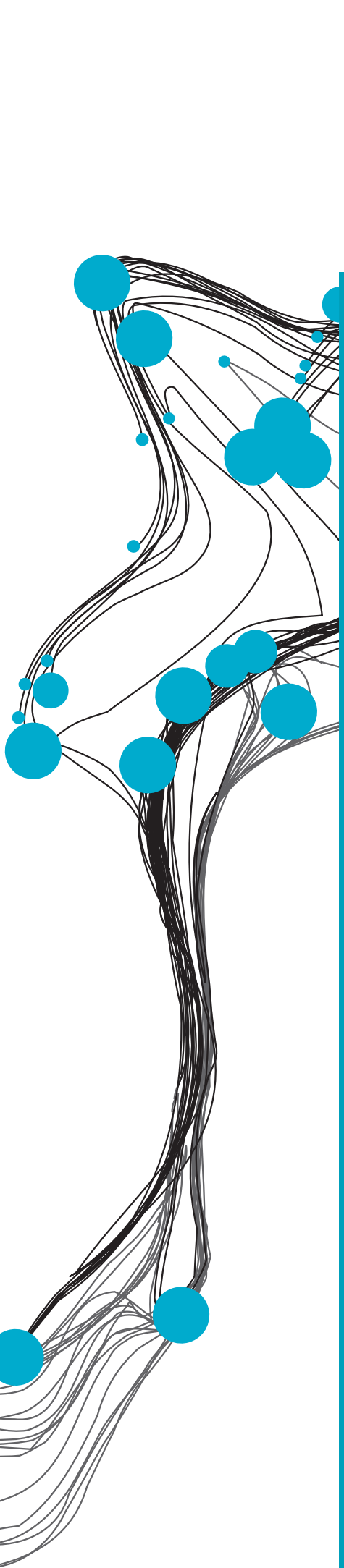

June 3, 2021

MASTER THESIS — APPLIED MATHEMATICS

Numerical time integration of stochastic differential equations

D. de Haan

Faculty of Electrical Engineering, Mathematics and Computer Science (EEMCS)

Chair: Multiscale Modeling and Simulation

Assessment committee:
Prof.Dr.Ir. B.J. Geurts
Dr. P.K. Mandal

Daily supervisor:
S. R. Ephrati

UNIVERSITY OF TWENTE.

Abstract

Time integration methods for stochastic differential equations are considered and compared for two models, namely the double pendulum and the Lagrangian drifter. The goal is to investigate how a choice in scheme has impact on the accuracy and correctness of the results. This is done by analysing the disturbance in the Poincaré sections for the double pendulum model, and using statistical tools for the model on the Lagrangian drifter. Two methods with a deterministic counter part of first order are considered, namely Euler-Maruyama and stochastic sympectic Euler, as well as two methods with deterministic counter part of a higher order, stochastic Störmer-Verlet and stochastic Runge-Kutta. The main result is that the result heavily relies on the type of model analysed. The stochastic Störmer-Verlet preserves the structure of the Poincaré section of the double pendulum better, and manages to preserve the total energy best. On the other hand, for the Lagrangian drifter the Euler-Maruyama method and the stochastic Runge-Kutta method yield generally identical dynamics.

Preface

Before you lies my master's thesis, the first of two big steps leading to the conclusion of my study of Applied Mathematics at the University of Twente.

Back in January of 2020, I discussed with Bernard Geurts, head of the chair Multiscale Modelling and Simulations, my plan for the final year as a student of Applied Mathematics in Enschede, starting in September. Back then I had 4 and a half blissful years of mathematics and student life behind me. We forged a plan which included an internship at Imperial College in London starting in September, which unfortunately got thrown over when the government of both the Netherlands as well as the United Kingdoms closed their borders due to the now well-established pandemic. Since then Bernard has always helped me look at options such that this final year would still be the icing on the cake, for which I am extremely grateful, as well as for the great guidance throughout the creation of this thesis.

Some more thanks are in order. First of all I want to thank Sagy for his help whenever necessary, for always standing open for discussions, as well as making good suggestions and helping with writing. Most of all I want to thank Sagy for the weekly Friday coffee meetings which we could have despite the current situation. I look forward to doing my internship with your guidance as well.

I want to thank the assessment committee for taking the time and effort to read and assess my work.

Final thanks are in order for people that are most dearest to me. Needless to say, I want to thank my parents and Rosa and Jarno, for being the most loving and supporting family. Without you I would not have stood were I am standing today.

Of course a thank you is in order to all my friends both here in Twente and back home, in the Noordoostpolder. You are making my time as a student here the most memorable time of my life, with numerous amazing moments to look back upon.

Finally, I would like to thank all the Henkies, for giving me the best home I could have wished for, especially during this past year.

Contents

Chapter 1

Introduction

In current days, ocean and climate change modelling has become very important to predict and combat the effects of the global climate change. Ocean modelling presents many significant challenges, caused by the complexity of the equations that describe it and the large range of dynamic scales involved. Small-scale influences, such as gusts of wind or changes in atmospheric pressure are typically not resolvable by computational models. This motivates an effective stochastic formulation to capture the nature of the dynamics. Stochastic noise is often added in models because there is uncertainty about parameters and initial - or boundary conditions, which may significantly alter the outcome of a model, or to compensate for missing information. A good example of the latter includes the study of "killer waves", where it is assumed that the undulation of waves can be described by stochastic processes, in [1]. Solving such *stochastic differential equations* analytically proves to be very difficult, motivating us to turn towards numerical methods to find approximations of these solutions. Stochastic time-integration is a subject of intense research [2]. We compare and develop such methods for canonical nonlinear systems, both with few degrees of freedom as in the stochastic double pendulum, as well as in problems with many degrees of freedom, as arise in shallow water models. The latter create a bridge between our investigations of stochastic time integration methods and the overarching interest in climate modeling.

Climate change has a significant impact on all human activities, as practical as wheat production in regions in China [3], but also in terms of increased variability of weather patterns [4] and issues of personal safety in relation to flooding [5, 6] and periods of severe droughts [7]. By creating comprehensive computational models, Science can contribute to the understanding of these mechanisms and to the design of measures to mitigate the consequences. The formulation of stochastic models to achieve reliable predictions of future developments, and which yields a quantification of the 'robustness' of the findings is a major approach towards this goal. The stochastic differential equation models require tailored numerical methods, in particular for the time integration. These methods and their performance is the main focus in this report. Apart from relevance for climate research, such stochastic modeling and simulation has various other uses. A good example includes the study of solute transport in porous media, see [8]. Also, the operation of future smart energy grids poses multiple challenges to stochastic time integeration that can also be answered using specific time integration methods.

The field of stochastic time-integration methods knows a long history. Starting from the seminal paper [9] by Maruyama, from which the Euler-Maruyama method is the earliest

example. Since numerical methods for stochastic differential equations are challenged by the fact that the noise has a direct relation on the convergence of the findings, current methods are of low order compared to deterministic systems. Important recent developments address the question whether and how underlying structures of the equations can be integrated entirely in the computational approach. Rather than aiming for higher order, these methods aim to preserve, e.g., a Hamiltonian structure, also in the discrete, stochastic implementation [10]. A motivating study in this direction may be found in [11]. Our primary aim in this research is to develop an understanding about how sensitive the quality of predictions depends on numerical details. For this purpose, the performance of various stochastic methods will be quantified in terms of the degree with which fundamental dynamical properties are represented, e.g., phase space patterns, and in terms of actual correspondence to scaling predictions, e.g., of dispersion properties, and correspondence to other high-fidelity simulations.

In this thesis, we compare several time integration methods in terms of stability and accuracy, by applying them to two mechanical models. The first is the model of the double pendulum, a set of ordinary differential equations describing the chaotic motion of this well-known example. The double pendulum is of interest since it enables a precise assessment of the quality of the numerical methods. We analyse the effect of the numerical method on the main structures seen in the Poincaré section, as well as in the actual time-evolving solution. In addition, we concentrate on the effect the noise has on main dynamical structures and on how well the energy in the system is conserved. We found that the stochastic Störmer-Verlet method showed promising results, keeping the shape of the Poincaré section more intact and keeping the value of the Hamiltonian over time approximately constant, also for stochastic perturbations.

The second model considered is the model of the Lagrangian Drifter, also known as Stokes' drift, in which point particles are released in an embedding velocity field, the latter of which is governed by a partial differential equation, for which we consider a shallow water model. Combined, the motion of the Lagrangian Drifters can be interpreted as the behaviour of a buoy on a large-scale ocean of shallow water. The expected value and variance of the locations of the drifters over time is analysed and compared to the expected value and variance of the analytic solution for an increasing amount of drifters. It is shown that different schemes show almost the same results in these terms, although the Euler-Maruyama method reaches this result with shorter running time.

The layout of this thesis is as follows:

- In chapter 2 we will give an introduction of the concepts used in the theory of stochastic differential equations (SDE's). We will introduce stochastic noise in the form of a Wiener process, and motivate this choice. The so-called Itô- and Stratonovich representations of an SDE are discussed, showing how the two closely related formulations are still different in interpretation. Finally, we will introduce the terms additive and multiplicative noise.
- In chapter 3, we introduce and analyse several time integration methods for SDE's. First, a motivation is given for using numerical methods to predict the behaviour of SDE's. Next, we will introduce the numerical methods used for our double pendulum and Lagrangian drifter. Methods to be discussed include the Euler-Maruyama and symplectic Euler method, both based on the first order Euler forward integrator. Furthermore, we will discuss two higher order Runge-Kutta methods and their stochastic counterparts. Next a discussion on the accuracy of a numerical method

for SDE's is given, as well as the definition of the strong order of a numerical method for an SDE, followed by an argument on what the effect of stochastic noise is on the order of a numerical method.

- In chapter 4 we test some of the previously mentioned methods for the double pendulum, with an additional stochastic term. We will first introduce the Hamiltonian formulation of the model and see that first order methods are unstable for this model. Next, we introduce the Poincaré section, to concisely characterize dynamic structures in phase space and facilitate comparison of methods.
- In chapter 5, we test the previously mentioned methods on the model of a drifter in a 1-dimensional flow enriched with a 2D noise perturbation. We analyse the dispersion of the drifters statistically for each method. Specifically, we measure the expected value and variance of the set of observations over time and check whether they converge towards the analytical expressions. Finally, we use this model to test for a velocity field with a physical representation.
- Finally, we conclude our findings in chapter 6.

Chapter 2

Introduction to Stochastic Differential Equations

This chapter introduces the theory necessary to analyse the numerical schemes introduced in chapter 3 and used in the chapters thereafter. Section 2.1 introduces the general notion of noise used in the model of the double pendulum and the Lagrangian drifter. Section 2.2 consecutively introduces the general notion of a stochastic differential equation using both the Itô and Stratonovich integral, and shows their difference in interpretation. Using these representations, we discuss how we can adjust the noise term by using additive or multiplicative noise, in section 2.3.

2.1 Wiener process

As mentioned in the introduction, we first need to state how we are going to add noise to our differential equations. A Wiener process is typically used in literature to describe the behaviour of natural phenomena such as the motion of a pollen emerged in water. This was explained by Albert Einstein as the effect of the water molecules pushing the pollen, see [12]. Examples of literature on a Wiener process can be found in [13, 14, 15].

Another way to look at stochastic differential equations known to the author is by the use of rough paths (e.g. [16]), which we will not consider, as this is not part of our scope.

We start by giving the formal definition of a Wiener process

Definition 2.1. *A stochastic process $W_t, t \geq 0$ is called a **Wiener process**, or **Brownian motion**, if it satisfies the following properties*

1. $W_0 = 0$.
2. *W has independent increments, i.e. $W_{t_3} - W_{t_2}$ is independent of $W_{t_2} - W_{t_1}$ for all $t_1 < t_2 < t_3$.*
3. *W has normally distributed increments, i.e. $W_{t_2} - W_{t_1} \sim \mathcal{N}(0, t_2 - t_1)$.*
4. *For almost all ω, the sample path $t \mapsto W_t(\omega)$ is continuous.*

Informally, a Wiener process can be seen as a representation for the integral of a Gaussian process. However, the derivative of a Wiener process does formally not exist, as discussed in [15].

2.2 Itô versus Stratonovich

In this paper we often refer to two representations of stochastic differential equations, namely Itô and Stratonovich. We will first show the representations in differential form to familiarise the reader with the notation, before we show how these two representations are different and how they come to be. We will follow with a discussion on the choice of representation.

An example we consider in this paper comes forward from sources that write a stochastic differential equation in Stratonovich form. Whenever we refer to such a representation, we write the differential equation in the following (differential) form

$$\mathrm{d}X = \underbrace{f(X)\mathrm{d}t}_{\text{Deterministic}} + \underbrace{g(X) \circ \mathrm{d}W_t}_{\text{Stochastic}}, \tag{2.1}$$

where $X = X(t)$ is a stochastic process, depending on time, which denotes the solution of equation 2.1. Notice that we do not write down $\frac{\mathrm{d}X}{\mathrm{d}t}$. This is due to the fact that the time derivative of a Wiener process W_t does not exist. We use the $\circ$-symbol to signal that we are using Stratonovich calculus. This is done in line with other literature on Stratonovich integrals, see for example [17, 13]. On the other hand, we refer to an Itô SDE whenever we write a differential equation in the (differential) form

$$\mathrm{d}X = \underbrace{f(X)\mathrm{d}t}_{\text{Deterministic}} + \underbrace{g(X)\mathrm{d}W_t}_{\text{Stochastic}}. \tag{2.2}$$

Itô and Stratonovich originate from different interpretations of the stochastic integral. First recall how the standard Riemann sum of an integral is defined. It estimates the area underneath a continuous function $f(t)$ on a (in)finite domain, e.g. $[0, T]$, as a sum of rectangles, bounded by the width of smaller intervals and the function itself. For example, if the height of the rectangles is determined to be equal to the value of $f(t)$ on the left side of the rectangles, the area underneath $f(t)$ is estimated by

$$\int_0^T f(t)\mathrm{d}t \approx \sum_{k=0}^{N-1} f(t_k)(t_{k+1} - t_k), \tag{2.3}$$

where $0 = t_0 < t_1 < \ldots < t_N = T$. If we take the height of the rectangles to be equal to the average value of f on the left and the right side of the rectangle, we get that the area underneath $f(t)$ is estimated by

$$\int_0^T f(t)\mathrm{d}t \approx \sum_{k=0}^{N-1} \frac{f(t_{k+1}) + f(t_k)}{2}(t_{k+1} - t_k). \tag{2.4}$$

Both equations (2.3) and (2.4) are good estimations of the area underneath $f(t)$ and for both we will have that the approximations become equalities if we let $N \to \infty$. However, when we integrate over a stochastic process, we cannot assure this equality anymore, which we will show. For example, let us consider the general example of an integral of a function f over a Wiener process:

$$\int_0^T f(W_t)\mathrm{d}W_t. \tag{2.5}$$

Itô [18] chose to approximate equation (2.5) by a left side approximation. This results in

$$\int_0^T f(W_t)\mathrm{d}W_t \approx \sum_{k=0}^{N-1} f(W_{t_k})(W_{t_{k+1}} - W_{t_k}). \tag{2.6}$$

Stratonovich [19], on the other hand, chose to approximate equation (2.5) by an approximation as in equation (2.4). This results in

$$\int_0^T f(W_t) \circ \mathrm{d}W_t \approx \sum_{k=0}^{N-1} \frac{f(W_{t_{k+1}}) + f(W_{t_k})}{2}(W_{t_{k+1}} - W_{t_k}). \tag{2.7}$$

Now taking the limit of N to infinity, we cannot assure that the two notations converge to the same limit, as the Brownian motion is a stochastic process. However, both are well posed options.

The choice in approach lies in the interpretation that one is mostly interested in. Both Itô and Stratonovich processes have their own advantages, like the Itô integral being a Martingale and the Stratonovich integral satisfying the ordinary chain rule of calculus. References include [14, 15]. Application-wise, the Itô formulation is often more popular in finance, while the Stratonovich formulation is more popular in physics.

In this paper, we will often start with a Stratonovich formulation of a set of stochastic differential equations, although numerical integration often requires Itô formulation. Fortunately, the Stratonovich stochastic processes can be converted to Itô stochastic processes and vice versa. To do so, we refer to theorem 2.2.

Theorem 2.2. *Let an Itô SDE be given by*

$$dX_t = f(X_t)dt + g(X_t)dW_t, \tag{2.8}$$

where $X_t \in \mathbb{R}^n$ denotes the state at time t. Furthermore assume that g is continuously differentiable. Then in integral form, the conversion to a Stratonovich SDE is given by

$$\int_0^T g(X_t)dW_t = \int_0^T g(X_t) \circ dW_t - \frac{1}{2}\int_0^T \frac{dg}{dx}(X_t)g(X_t)dt \tag{2.9}$$

Proof. See appendix A. □

More generally, by taking the derivatives of each term in equation (A.6), we can also write the conversion in differential form.

Corollary 2.2.1. *Let an Itô SDE be given by equation* (A.5)*, where $f, g : \mathbb{R}^n \to \mathbb{R}^n$. Then in differential form, a Stratonovich SDE is given by*

$$dX_t = \left(f(X_t) - \frac{1}{2}c(X_t)\right)dt + g(X_t) \circ dW_t, \tag{2.10}$$

where $c : \mathbb{R}^n \to \mathbb{R}^n$ is given by

$$c^i(X_t) = \sum_{j=1}^{k} \frac{dg^i}{dx_j}(X_t)g^j(X_t), \forall i = 1, \ldots, n.$$

2.3 Types of noise

There are two main archetypes of noise which are considered when analysing stochastic integrals, namely additive noise and multiplicative noise. For that purpose, let us look at the Itô formulation of a stochastic differential equation, equation (2.2). The type of noise is fully determined by the function $g(X)$.

We say that the noise in the stochastic differential equation is additive if we have that $g(X) = \beta$, where $\beta \in \mathbb{R}$ is a constant. Notice that for additive noise, we have that the Itô and Stratonovich differential form are identical, following directly from theorem 2.2. If we have no additive noise, i.e. $g(X)$ is a function of the state X, we say that the noise is multiplicative.

Both additive and multiplicative noise are recognised in several applications. See for example [20].

2.4 Summary

In this chapter we have introduced the general notion of a Wiener process and its uses in stochastic differential equations. Two interpretations of the stochastic integral were introduced, those of Itô and Stratonovich. Additive and multiplicative noise were introduced as well as the consequences of these types of noise on the stochastic integral using the mentioned interpretations. These newly introduced results allow us to formulate stochastic differential equations. Furthermore, these terms will be used when considering solutions for the double pendulum and Lagrangian drifter models in chapters chapter 4 and chapter 5.

Chapter 3

Time integration methods

In this chapter we will translate the general stochastic differential equation introduced in chapter 2 to a numerical model. The numerical methods introduced in this section are the Euler-Maruyama method, the stochastic Runge-Kutta method, the stochastic symplectic Euler method and the stochastic Störmer-Verlet method, which are the methods to be used in chapters 4 and 5. Section 3.1 introduces the general notion of a numerical method for stochastic differential equations and discusses the requirements of a numerical scheme to be applicable to stochastic differential equations. Section 3.2 display the specific methods used. Finally in section 3.3, we introduce the notion of weak and strong order of convergence of the numerical schemes, and discuss why the analysis for numerical methods for stochastic differential equations is more difficult than for deterministic schemes.

3.1 Why use numerical methods

Let us again consider a general model of an Itô representation of a stochastic differential equation:

$$\mathrm{d}X = f(X)\mathrm{d}t + g(X)\mathrm{d}W_t. \tag{3.1}$$

In integral form, we can find that the solution $X(t)$ to equation (3.1) is given by

$$X(t) = X(t_0) + \int_{t_0}^{t} f(X(s))\mathrm{d}s + \int_{t_0}^{t} g(X(s))\mathrm{d}W_s, \tag{3.2}$$

where $0 \leq t_0 < T$ are the initial and final time of the model, respectively. Computing this can become very difficult quickly for nonlinear functions f and g, and computational wise it could be very inefficient.

Simultaneously, in chapter 4 we will consider an even-dimensional system $X(t) = (q(t), p(t))^\top$. This, we can write into the set of differential equations,

$$\begin{aligned} \mathrm{d}q &= f(q,p)\mathrm{d}t + \sigma(q,p)\mathrm{d}W_t \\ \mathrm{d}p &= g(q,p)\mathrm{d}t + \gamma(q,p)\mathrm{d}W_t. \end{aligned} \tag{3.3}$$

The notation used here is in line with [21], where the symplectic integration of Hamiltonian systems is considered. As mentioned in the reference, the symplectic structure is only preserved if there exist functions $H(q,p)$ and $h(q,p)$ such that $f = \frac{\partial H}{\partial p}$ and $g = -\frac{\partial H}{\partial q}$, as well as $\sigma = \frac{\partial h}{\partial p}$ and $\gamma = -\frac{\partial h}{\partial q}$.

In the same fashion as equation (3.2), we can find that the solution $(q(t), p(t))$ to equation (3.1), in integral form, is given by

$$\begin{aligned} q(t) &= q(t_0) + \int_{t_0}^{t} f(q(s), p(s))\mathrm{d}s + \int_{t_0}^{t} \sigma(q(s), p(s))\mathrm{d}W_s \\ p(t) &= p(t_0) + \int_{t_0}^{t} g(q(s), p(s))\mathrm{d}s + \int_{t_0}^{t} \gamma(q(s), p(s))\mathrm{d}W_s. \end{aligned} \tag{3.4}$$

where $0 \leq t_0 < T$ are the initial and final time of the model, respectively. We again have an expression similar to that in equation (3.1), which we could argue again is hard and inefficient to compute. This motivates us to turn towards numerical methods to approximate the solutions of these stochastic differential equations.

3.2 Methods

In this we introduce four numerical methods which we will use to approximate the solution $X(t)$ as introduced in section 3.1 over time. We will introduce a few specifics of the methods possible, but refer the reader to many more possible methods which can be found in e.g. [22, 23, 17].

The methods chosen all have been chosen with the models in chapters 4 and 5 in mind. Specifically, we chose four methods that all have a known deterministic counterpart, because these deterministic methods are known to be suitable for the deterministic versions of the upcoming two models.

We have chosen in the following sections to use a constant time step size Δt, to make the schemes more easy to read, but also as we will be using a constant time step sizes in the models in the following chapters, to simplify the implementation as well as the analysis of these models.

Euler-Maruyama

The first of the considered time integration methods is one of the simplest approximations of an Itô process, called the Euler-Maruyama method [9]. It is an extension of the first order explicit Euler method. This method is chosen due to its simplicity in interpretation. This method was the first numerical stochastic time integration method considered after the analysis done by Itô in 1944, and approximates a solution of problem equation (3.1). The method is given by:

$$X_{n+1} = X_n + f(X_n)\Delta t + g(X_n)\Delta W_t \tag{3.5}$$

Stochastic Runge-Kutta

The stochastic scheme based on the fourth order Runge-Kutta method is constructed in [23]. There are many more Runge-Kutta schemes, the one chosen here is the most in line

with the fourth order deterministic Runge-Kutta scheme. The method is given by:

$$\begin{aligned} k_1 &= f(X_n)\Delta t + g(X_n)\Delta W_t \\ k_2 &= f(X_n + k_1/2)\Delta t + g(X_n + k_1/2)\Delta W_t \\ k_3 &= f(X_n + k_2/2)\Delta t + g(X_n + k_2/2)\Delta W_t \\ k_4 &= f(X_n + k_3)\Delta t + g(X_n + k_3)\Delta W_t \\ X_{n+1} &= X_n + \frac{1}{6}(k_1 + 2k_2 + 2k_3 + k_4). \end{aligned} \tag{3.6}$$

Here, $k_1, \ldots, k_4$ are the internal stages of the stochastic Runge-Kutta method.

Stochastic symplectic Euler

The following method approximates a solution for equation (3.3) and is based on its deterministic counterpart. This method is introduced in [21], but is also analysed in [17]. The method is given by:

$$\begin{aligned} q_{n+1} &= q_n + f(q_{n+1}, p_n)\Delta t + \sigma(q_{n+1}, p_n)\Delta W_t, \\ p_{n+1} &= p_n + g(q_{n+1}, p_n)\Delta t + \gamma(q_{n+1}, p_n)\Delta W_t \end{aligned} \tag{3.7}$$

Stochastic Störmer-Verlet

The final method also approximates a solution for equation (3.3). Based on the deterministic Störmer-Verlet scheme, it calculates an extra internal stages compared to the stochastic symplectic Euler method. The method is given by: [17]

$$\begin{aligned} p_{n+1/2} &= p_n + \frac{1}{2}g(q_n, p_{n+1/2})\Delta t + \frac{1}{2}\gamma(q_n, p_{n+1/2})\Delta W_t \\ q_{n+1} &= q_n + \frac{1}{2}\left(f(q_n, p_{n+1/2}) + f(q_{n+1}, p_{n+1/2})\right)\Delta t + \frac{1}{2}\left(\sigma(q_n, p_{n+1/2}) + \sigma(q_{n+1}, p_{n+1/2})\right)\Delta W_t \\ p_{n+1} &= p_n + \frac{1}{2}g(k_{n+1}, p_{n+1/2})\Delta t + \frac{1}{2}\gamma(q_{n+1}, p_{n+1/2})\Delta W_t. \end{aligned} \tag{3.8}$$

Here, we solve the first two steps of the method iteratively and calculate the final step explicitly.

3.3 Convergence of a stochastic numerical method

In this section we introduce the notion strong order of convergence for a numerical method, and elaborate on the order of convergence of the Euler-Maruyama method. We want to show that a numerical method for an SDE generally converges slowly towards the solution, motivating us to turn to other quantities to check the performance of a method.

The order of convergence is a quantities that shows how close the true solution $X(t)$ from equation (3.2) or equation (3.4) lies towards the estimated solution, for now called $Y(t)$, found using a numerical method. It can be shown for both the Euler-Maruyama and the stochastic Runge-Kutta method that these methods have a low order of convergence. The theory discussed here is in line with that given in [13].

In stochastic differential equations, there are two different interpretations of the order of convergence. These are called weak and strong convergence, and the difference here lies

in the use of the expected value, or the mean. If we take the mean of the difference between the exact solution $X(t)$ and the estimated solution $Y(t)$, we would talk about strong convergence. On the other hand, looking at the difference between the mean of the exact solution $X(t)$ and the mean of the estimated solution $Y(t)$ would be the notation for weak convergence. The strong order of convergence is what we use to compare the order of convergence of a stochastic numerical method with the order of a deterministic numerical method, and thus is the notation of interest here.

Formally, we say that a time discrete approximation Y^δ with maximum step size δ converges strongly to X with order $\gamma > 0$ at time T if there exists a positive constant C, which does not depend on δ, and a $\delta_0 > 0$ such that

$$\epsilon(\delta) = \mathrm{E}(|X_T - Y^\delta(T)|) \leq C\delta^\gamma \tag{3.9}$$

for each $\delta \in (0, \delta_0)$.

From [13], we know that the Euler-Maruyama scheme has a strong order of 0.5 for an SDE. Similarly, the stochastic Runge-Kutta method given by equation (3.6) has order 0.5 as well. [23].

The order of convergence of a stochastic differential equation is in general low, as could be seen by the two examples. The addition of a stochastic variable has the effect that deterministic high order schemes such as the fourth order Runge-Kutta scheme diminishes in order. This motivates to look at different quantities to investigate, such as preservation of energy, which we will look at in chapter 4.

3.4 Implementation

In chapters 4 and 5 we will look at the methods introduced in this chapter. The implementation of these numerical methods is done using MATLAB.

The value of Δt has a direct relation to the variance of the Wiener process. Although we could choose Δt very large to minimise the frequency with which we add noise, this would also imply that the noise becomes bigger, such that there will effectively be no difference. Hence in each model we will choose an amplification factor β which we will multiply with the Wiener process, such that we still can have influence on the size of the noise, and choose for each model a time step size Δt that is suitable for the deterministic version of the respective model.

The computational cost of the four methods are all different. The stochastic Runge-Kutta methods, compared to the Euler-Maruyama method, uses three extra steps during one iteration to compute the next value of X_{n+1}. For these two methods, all of these calculations are explicit. Furthermore, the stochastic symplectic Euler method only uses two steps, but the first step is implicit, which is calculated using an iterative solver, namely the Newton method. The stochastic Störmer-Verlet method has two implicit steps and one explicit step, making it the slowest computational method. Here the implicit steps are also calculated using the Newton method.

Chapter 4

Stochastic Double Pendulum

In this chapter we study the stochastic double pendulum to get acquainted with several schemes introduced in the previous chapter. Section 4.1 describes the basic dynamical system of a double pendulum, and tells why this problem is of importance. This is followed by section 4.2, where the Hamiltonian formulation for the double pendulum is derived, followed by an analysis regarding the stability of several numerical schemes designed for this system. This analysis is then used to show that the Euler-Maruyama and Milstein methods are not well-suited for this problem. Section 4.4 describes how a Poincaré section can be set up for the double pendulum and shows some characteristic dynamic structures for the deterministic system. In section 4.5, the Poincaré sections are shown for the stochastic problem using the stochastic Störmer-Verlet and stochastic symplectic Euler method. We show the difference in results of these methods in both the Poincaré sections as well as the energy level of the system. This is done for Stratonovich multiplicative noise.

4.1 Introduction to the double pendulum

The double pendulum is a system that has been under study for centuries, with some of the oldest references found in [24]. Several decades ago, chaotic non-linear systems like the double pendulum were of high interest due to the rise of computational simulations. An example of the simulation of a driven damped pendulum can be found in [25]. Because the behaviour has been analysed thoroughly and the equations are well described, we can use this as a good place to start introducing noise and testing the time integration methods. More importantly, the sum of energies acting on the double pendulum is constant over time. This motivates to describe the model as a Hamiltonian system. An important feature is that it is unknown whether the system stays Hamiltonian, i.e., preserves energy (on average), for each of the numerical methods that we chose. We will come back to this question in section 4.3. The next section describes the deterministic system as a Hamiltonian, in which we will introduce noise later on.

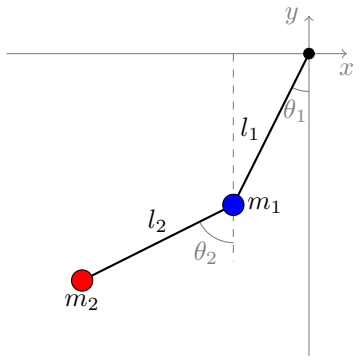

Figure 4.1: Schematic representation of a double pendulum.

4.2 Equations of motion

We describe the system as a Hamiltonian system to reflect the energy conservation of the system. In appendix B, the derivation of the Hamiltonian can be found.

$$H(\theta_1,\theta_2,p_{\theta_1},p_{\theta_2}) = \frac{l_2^2 m_2 p_{\theta_1}^2 + l_1^2\left(m_1+m_2\right)p_{\theta_2}^2 - 2m_2 l_1 l_2 p_{\theta_1} p_{\theta_2}\cos\left(\theta_1-\theta_2\right)}{2l_1^2 l_2^2 m_2\left[m_1+\sin^2\left(\theta_1-\theta_2\right)m_2\right]} \\ -(m_1+m_2)gl_1\cos(\theta_1) - m_2 g l_2\cos(\theta_2). \tag{4.1}$$

Here, we have defined the following variables and parameters:

- θ_1, θ_2: the angle of the first and second pendulum, respectively.
- $p_{\theta_1}, p_{\theta_2}$: the canonical momentum of the first and second pendulum, respectively.
- m_1, m_2: the masses of the first and second pendulum, respectively.
- l_1, l_2: the length of the rods of the first and second pendulum, respectively.
- g: the gravitational constant.

We can now find the characteristic equation describing the change in time of both the angles, as well as the canonical momenta. The update of each of the variables over time is given by

$$\begin{aligned}
\dot{\theta}_1 &= \frac{\partial H}{\partial p_{\theta_1}} = \frac{l_2 p_{\theta_1} - l_1 p_{\theta_2}\cos\left(\theta_1-\theta_2\right)}{l_1^2 l_2\left[m_1+m_2\sin^2\left(\theta_1-\theta_2\right)\right]} \\
\dot{\theta}_2 &= \frac{\partial H}{\partial p_{\theta_2}} = \frac{l_1\left(m_1+m_2\right)p_{\theta_2} - l_2 m_2 p_{\theta_1}\cos\left(\theta_1-\theta_2\right)}{l_1 l_2^2 m_2\left[m_1+m_2\sin^2\left(\theta_1-\theta_2\right)\right]} \\
\dot{p}_{\theta_1} &= -\frac{\partial H}{\partial \theta_1} = -\left(m_1+m_2\right)gl_1\sin\theta_1 - K_1 + K_2 \\
\dot{p}_{\theta_2} &= -\frac{\partial H}{\partial \theta_2} = -m_2 g l_2\sin\theta_2 + K_1 - K_2,
\end{aligned} \tag{4.2}$$

where K_1 and K_2 are equal to

$$\begin{aligned}
K_1 &\equiv \frac{p_{\theta_1}p_{\theta_2}\sin\left(\theta_1-\theta_2\right)}{l_1 l_2\left[m_1+m_2\sin^2\left(\theta_1-\theta_2\right)\right]} \\
K_2 &\equiv \frac{l_2^2 m_2 p_{\theta_1}^2 + l_1^2\left(m_1+m_2\right)p_{\theta_2}^2 - l_1 l_2 m_2 p_{\theta_1}p_{\theta_2}\cos\left(\theta_1-\theta_2\right)}{2l_1^2 l_2^2\left[m_1+m_2\sin^2\left(\theta_1-\theta_2\right)\right]^2}\sin\left[2\left(\theta_1-\theta_2\right)\right].
\end{aligned} \tag{4.3}$$

Here we indicate the time derivatives of each variable in equation (4.13) with a dot, i.e., $\dot{x} = \frac{\mathrm{d}x}{\mathrm{d}t}$. We now have a set of four ordinary differential equations which can be solved using a numerical time integration method.

4.2.1 Stochastic equations

We want to investigate how we can use time integration methods for a stochastic differential equation. Since the double pendulum does not involve any stochastic variables, we add noise as considered in chapter 2. Specifically, we decide to add Stratonovich noise to the canonical momenta. This is done in line with the theory mentioned in [17, 10]. This also makes sense to do so here, due to the fact that adding noise to the angles could violate basic dynamics of the system. What we mean by this is that the angles of the two pendula could reach a state such that the distance between the two pendula changes, i.e., the distance would not equal the initial l_2 anymore.

Furthermore, linear multiplicative noise is analysed, that is, we multiply the noise added to the canonical momentum by their respective angle. We do this, as multiplicative Stratonovich noise is of most interest in chapter 5. The equations for the canonical momenta with additional noise are given by

$$\begin{aligned} \mathrm{d}p_{\theta_1} &= \underbrace{-\frac{\partial H}{\partial \theta_1}\mathrm{d}t}_{\text{Deterministic}} \underbrace{-\beta\theta_1 \circ \mathrm{d}W}_{\text{Stochastic}} \\ \mathrm{d}p_{\theta_2} &= \underbrace{-\frac{\partial H}{\partial \theta_2}\mathrm{d}t}_{\text{Deterministic}} \underbrace{-\beta\theta_2 \circ \mathrm{d}W}_{\text{Stochastic}}, \end{aligned} \tag{4.4}$$

where we again use the notation as explained in chapter 2. In these equations, β is a (small) parameter which we will use to control the amount of noise added to the system. Since $\theta_{1,2}$ are angles, we will use their periodicity to keep them inside the interval $[-\pi, \pi\rangle$. We will do this to ensure that both the $\beta\theta$ terms in equation (4.4) do not get too large, which would lead to a larger impact from the noise term and could spiral the system out of control.

Note that the noise added in equation equation (4.4) could cause the energy in the system to vary over time. This has to be kept in mind as the system would no longer be a Hamiltonian system. Nevertheless, we could still simulate the system over time and see the effect the noise has on the total energy in the system. We will do so in section 4.4 and discuss the relevance of the result.

4.2.2 Parameter values in simulations

The values of the parameters in equation (4.1) for the simulations are chosen to be

- $(m_1, m_2) = (2, 1)$,
- $(l_1, l_2) = (1, 1)$,
- $g = 9.81$.

The length of both pendula are chosen to be equal such that the analysis done in section 4.3 is simplified. Typically, these values are chosen to be equal to one, to provide a simple example (see e.g. [26]), which is why we choose them to be equal to one here as well.

The value of the second mass has been chosen to be equal to one, by the same reasoning. Furthermore the value for g is chosen such that it is in line with the gravitational constant on earth. These parameters also have the effect that the minimal value of the Hamiltonian equals $-4g \approx -39$, corresponding to the value of the Hamiltonian if both pendula are pointing down ($(\theta_1, \theta_2) = (0, 0)$).

The numerical implementation adopts a time step size $\Delta t = 0.01$. This value ensures both fast computational time for a long run, while retaining accuracy. The effect on the results by increasing this value and their significance will be discussed in section 4.6.

4.2.3 How to compare results

We want to find a suitable method to compare the numerical schemes used in this chapter. To do so, we introduce three levels of detail. The most detailed level would be comparing each of the variables over time. This is done for the first 10 seconds. In our final results, we will increase this simulation time significantly. However this short simulation already gives a good impression. For longer simulations the results quickly differ and large local errors accumulate. Here we have chosen parameters in line with section 4.2.2. This includes a time step size of $\Delta t = 0.01$. We have also slightly varied this value, which only influences the time before a local difference between the methods comes to be.

Figure 4.2 shows four plots illustrating the time evolution of all solution components. The initial correspondence of the different methods is seen to be lost quite soon and all detailed local comparison at this finest level is not so relevant anymore.

We introduce the next level of comparison, by zooming out of the individual behaviour of each of the variables, and looking at the behaviour of the model by showing the trajectory the two pendula follow. In figure 4.3, the first few seconds of running time for the deterministic methods can be seen.

Figure 4.3 shows that the Euler forward method behaves quite different after a short run. This leads us to question the numerical stability of this scheme, which will be analysed in section 4.3. Furthermore, figure 4.3 shows that it is difficult to compare and draw conclusions on the behaviour of the trajectory in physical space itself already after a few seconds. Moreover, the comparison should clearly show the influence of noise after a long run, because we are mostly interested in the dynamic effect of noise. This leads to the third and coarsest level of detail, which is displaying the dominant dynamical structures in terms of the Poincaré section of the double pendulum. See section 4.4 for an introduction on the theory of Poincaré sections, as well as examples for the deterministic Störmer-Verlet and symplectic Euler method. We will frequently use Poincaré sections in the sequel of this report.

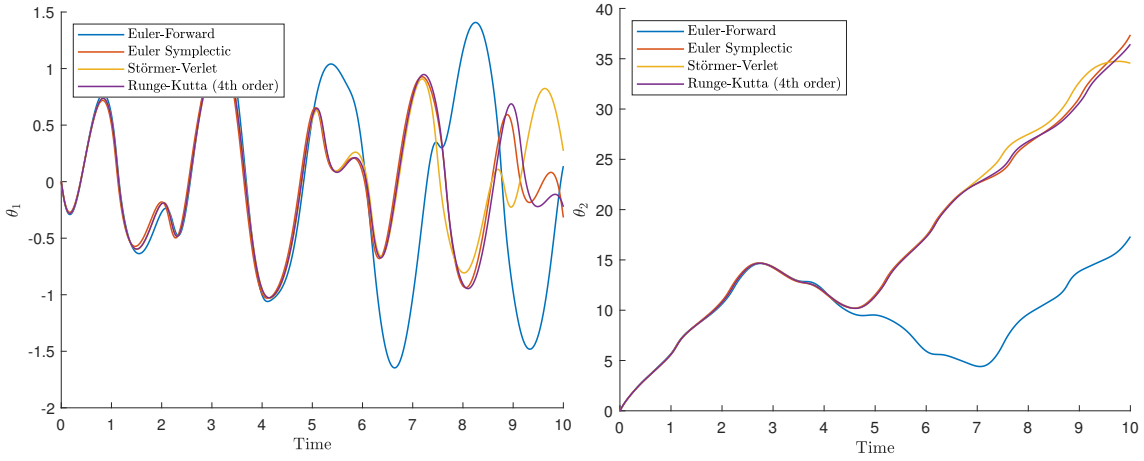

(a) θ_1 over time.

(b) θ_2 over time.

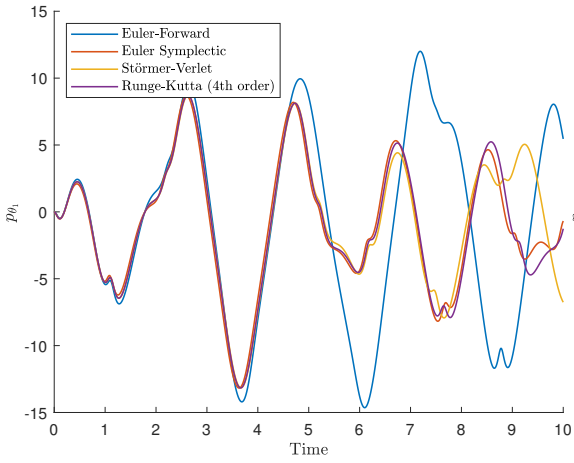

(c) p_{θ_1} over time.

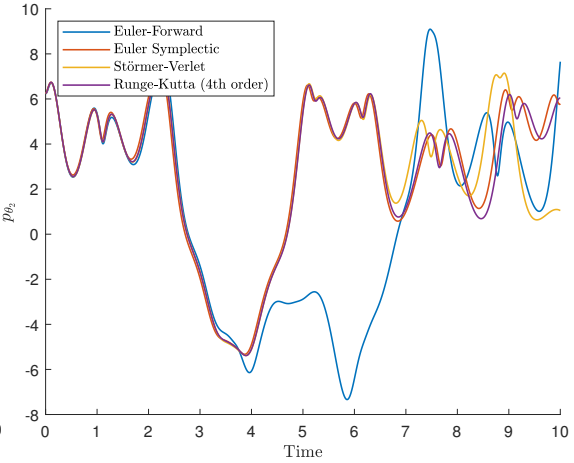

(d) p_{θ_2} over time.

Figure 4.2: Behaviour of all four variables over time, for a short run of the double pendulum using 4 different numerical methods. The Euler-Forward method shows a qualitatively different outcome compared to the other three methods, which seem to stay very close to each other for a much longer time.

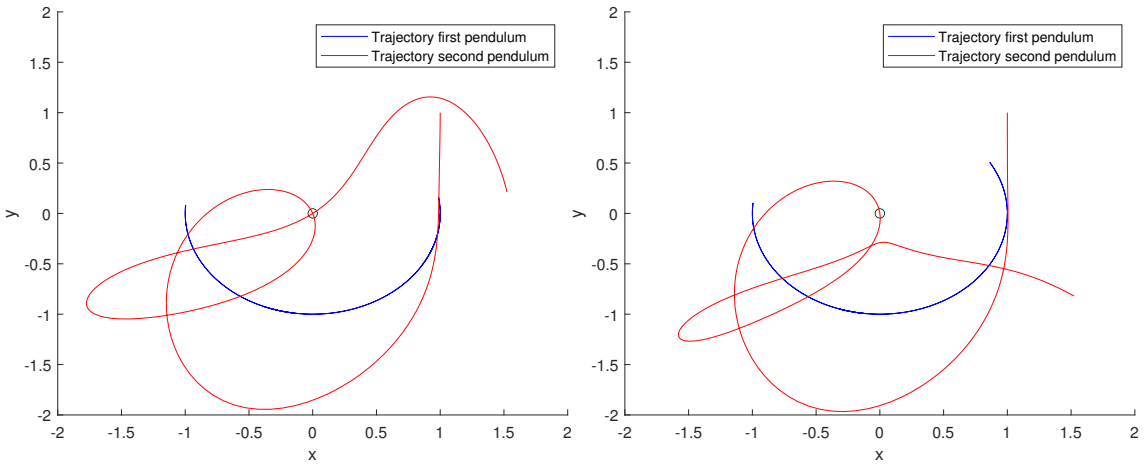

(a) Euler Forward.

(b) Classic Runge-Kutta 4.

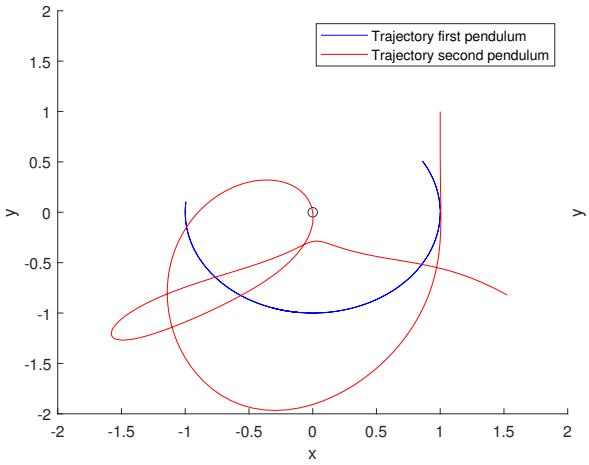

(c) Störmer-Verlet.

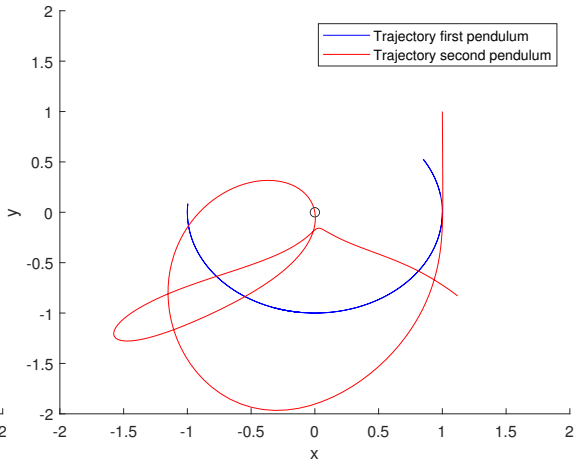

(d) Symplectic Euler.

Figure 4.3: Short run of the double pendulum using 4 different methods. In a few seconds of running time, the Euler forward method already shows a significantly different outcome. The Runge-Kutta and Störmer-Verlet trajectories seem identical from this perspective, as is the symplectic Euler method. The comparison of trajectories in space does not allow to discuss great detail and is hard to interpret.

4.3 Justifying the numerical methods

It is desirable that the deterministic variant of the time integration methods considered conserve the value of the Hamiltonian. For this purpose, we analyse the numerical stability of each proposed scheme for the model of the double pendulum, in line with [27]. To do so, the eigenvalues of the double pendulum model are found and used to determine whether a numerical scheme is stable for this system. We will show that the eigenvalues are imaginary, which implies that the Euler explicit method and its stochastic counterparts are unstable methods for this problem as is established in [28].

Since the Hamiltonian is nonlinear, analysis regarding the eigenvalues of the system can be quite difficult. To simplify, the system is linearized around $(\theta_1, \theta_2) = (0, 0)$. For small angles, the partial derivatives of the Lagrangian are approximated by

$$\begin{aligned} \frac{\partial L}{\partial \theta_1} &= -(m_1 + m_2) l_1 g \theta_1 \\ \frac{\partial L}{\partial \theta_2} &= -m_2 l_2 g \theta_2 \\ \frac{\partial L}{\partial \dot{\theta_1}} &= (m_1 + m_2) l_1^2 \dot{\theta_1} + m_2 l_1 l_2 \dot{\theta_2} \\ \frac{\partial L}{\partial \dot{\theta_2}} &= m_2 l_2^2 \dot{\theta_2} + m_2 l_1 l_2 \dot{\theta_1} \end{aligned} \tag{4.5}$$

We want to use the Euler-Lagrange equation (equation (B.8)) to find the eigenvalues of the system. The equality that follows is given by

$$\begin{aligned} -(m_1 + m_2) l_1 g \theta_1 &= (m_1 + m_2) l_1^2 \ddot{\theta_1} + m_2 l_1 l_2 \ddot{\theta_2} \\ -m_2 l_2 g \theta_2 &= m_2 l_2^2 \ddot{\theta_2} + m_2 l_1 l_2 \ddot{\theta_1} \end{aligned} \tag{4.6}$$

This can be written in matrix form as

$$A \begin{bmatrix} \theta_1 \\ \theta_2 \end{bmatrix} + B \begin{bmatrix} \ddot{\theta_1} \\ \ddot{\theta_2} \end{bmatrix} = 0, \tag{4.7}$$

where

$$\begin{aligned} A &= \begin{bmatrix} (m_1 + m_2) l_1 g & 0 \\ 0 & m_2 l_2 g \end{bmatrix} \\ B &= \begin{bmatrix} (m_1 + m_2) l_1^2 & m_2 l_1 l_2 \\ m_2 l_1 l_2 & m_2 l_2^2 \end{bmatrix}. \end{aligned} \tag{4.8}$$

A general solution is of the form

$$\begin{bmatrix} \theta_1 \\ \theta_2 \end{bmatrix} = \begin{bmatrix} E_1 \\ E_2 \end{bmatrix} e^{\lambda t}, \tag{4.9}$$

where λ are the eigenvalues of our system, and E_1 and E_2 are the eigenvectors of the system. Filling in this solution, we find that the eigenvalues satisfy the following equality:

$$\det\left(A + \lambda^2 B\right) = 0. \tag{4.10}$$

Solving this for λ yields

$$(m_1 + m_2)\, g^2 - \lambda^2 (m_1 + m_2)(l_1 + l_2)\, g + \lambda^4 m_1 l_1 l_2 = 0. \tag{4.11}$$

We now restrict ourselves towards the situation $l_1 = l_2 = l$. In this case, the solution for λ is given by

$$\lambda_{1,2}^2 = -\frac{g}{l}\left(1 + \frac{m_1}{m_2} \pm \sqrt{\frac{m_1}{m_2}\left(1 + \frac{m_1}{m_2}\right)}\right). \tag{4.12}$$

Since it is assumed that all above parameters are positive constants, this equations results in two negative values for $\lambda_{1,2}^2$. Specifically, it follows that all four eigenvalues of the system of a double pendulum are imaginary.

We can refer to many books on analysis of numerical methods (see e.g. [27]) to immediately state that the Euler forward method is unstable for a system consisting of imaginary eigenvalues. The reason can be investigated using [28]. Hence, this method is not suited as a solver for the model of the double pendulum. This result is further supported by plotting the value of the Hamiltonian over time for non-specific initial conditions. This can be found in figure 4.4. Here we look at initial value $H = -10$, which can be seen as a typical case of high energy. Indeed the Störmer-Verlet and fourth order Runge-Kutta method remain stable, while the Euler forward method does not. From this, it can be concluded that the Euler-Maruyama method is an unsatisfactory method to use for this problem. Consequently, we decide to use the stochastic symplectic Euler method instead, which does conserve energy and has a deterministic counterpart that is first order.

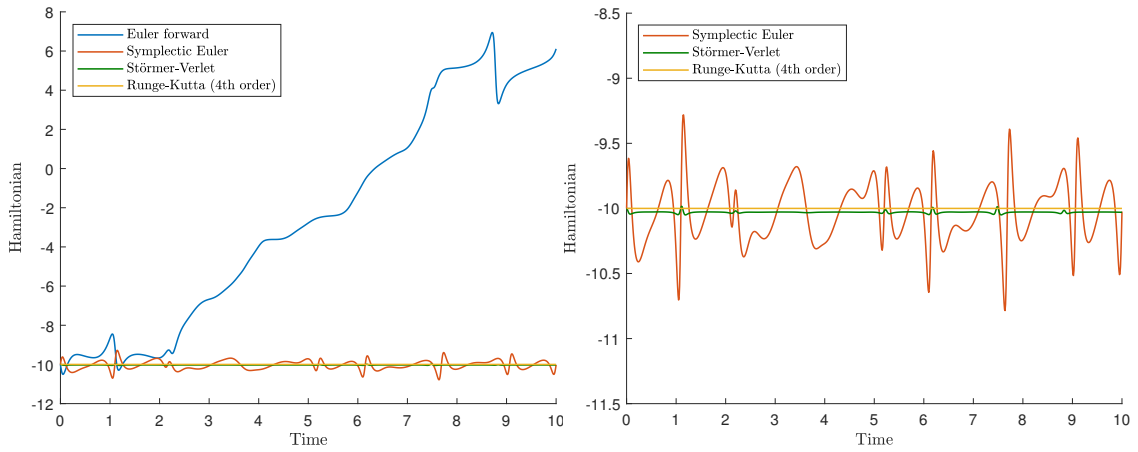

(a) Hamiltonian including Euler-Forward. (b) Hamiltonian excluding Euler-Forward.

Figure 4.4: Energy levels of the four methods. The energy for the Euler forward method increases over time, for the Störmer-Verlet and fourth order Runge-Kutta method it stays generally constant.

Figure 4.4 shows that the result from the Runge-Kutta fourth order method and the Störmer-Verlet method is very similar, which is in line with the result in figure 4.3. This peaks our interest in comparing the Störmer-Verlet and the Symplectic Euler method in an efficient way to detect structure in the model of the double pendulum.

4.4 Deterministic Poincaré section

In this section we will show a Poincaré section for the double pendulum, for several levels of energy. All results in this section are obtained using the Störmer-Verlet method, which has shown to be both efficient and robust. Due to the fact that there are more periodic orbits of the double pendulum at low energy levels, we will restrict ourselves to these levels. After showing the Poincaré sections for the deterministic system, we will add Stratonovich multiplicative noise in the next session and examine the results of the implementation using the stochastic Störmer-Verlet and stochastic symplectic Euler method.

The Poincaré section is a tool often used to find structure in a (chaotic) dynamical system. Their concept were named after Henri Poincaré, based on his research in and around 1892 [29]. For the double pendulum, the Poincaré map has been used before to determine stable orbits for the double pendulum [30, 31]. The basic idea of the Poincaré section is to map our four-dimensional system onto a two-dimensional plane. This plane should be chosen such that it is transversal with the flow, i.e., such that the points move through the chosen plane [30]. We consider one Poincaré section, namely the one at $\theta_1 = 0$ with a positive velocity $\dot{\theta}_1$. This section is chosen in line with several other papers [30, 31], but was also chosen due to its many clear sections that were found.

To show the usefulness of the Poincaré sections, a Poincaré section at $H = -10$ is shown in figure 4.5. The value of the Hamiltonian is chosen such that we observe a high energy level, for which $H = -10$ is a typical case. Here we chose the parameter values as discussed in section 4.2.2. The grey shattered dots indicate chaos, while the three coloured regions show periodic orbits. For example, if we now choose initial conditions in the centre of the blue region shown in figure 4.5, we get the periodic orbit as shown in the right picture.

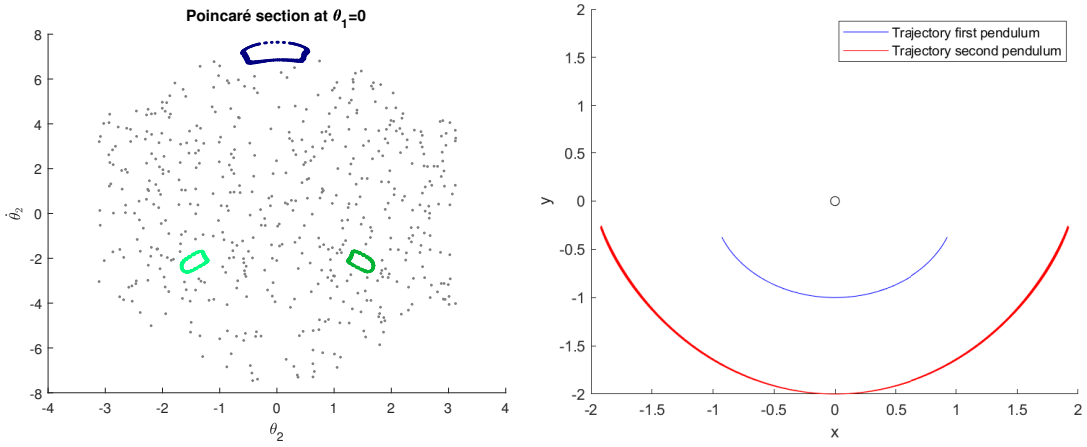

(a) Poincaré section.

(b) Periodic orbit found at the centre of the blue orbit shown in the Poincaré section.

Figure 4.5: Poincaré section for a high energy level $H = -10$, together with a periodic orbit. Each of the coloured region in the Poincaré sections indicates a separate initial condition. Upon closer inspection, it seems like there are more spots where periodic orbits could be found. However, investigating initial conditions in these empty spots did not result in more periodic orbits, rather again in chaotic trajectories. The boundary resembles a hexagon, which means that the extreme values of position and velocity of the second pendulum are limited. Finally the behaviour of the blue orbit is considerably more simple than the behaviour of the two green orbits, which show a more complex trajectory.

Now that we have a first impression of our Poincaré section, we decrease the value of the Hamiltonian such that more periodic orbits are obtained inside our Poincaré section. In figure 4.6, the effect of lowering the energy level can be seen. As the energy decreases, we see more orbits being created until we can find many at $H = -20$. As this energy level contains a high number of periodic orbits that could be found, we decide to not decrease the value of the Hamiltonian any further. Instead, the influence of stochastic noise on the time integration method at this energy level is studied.

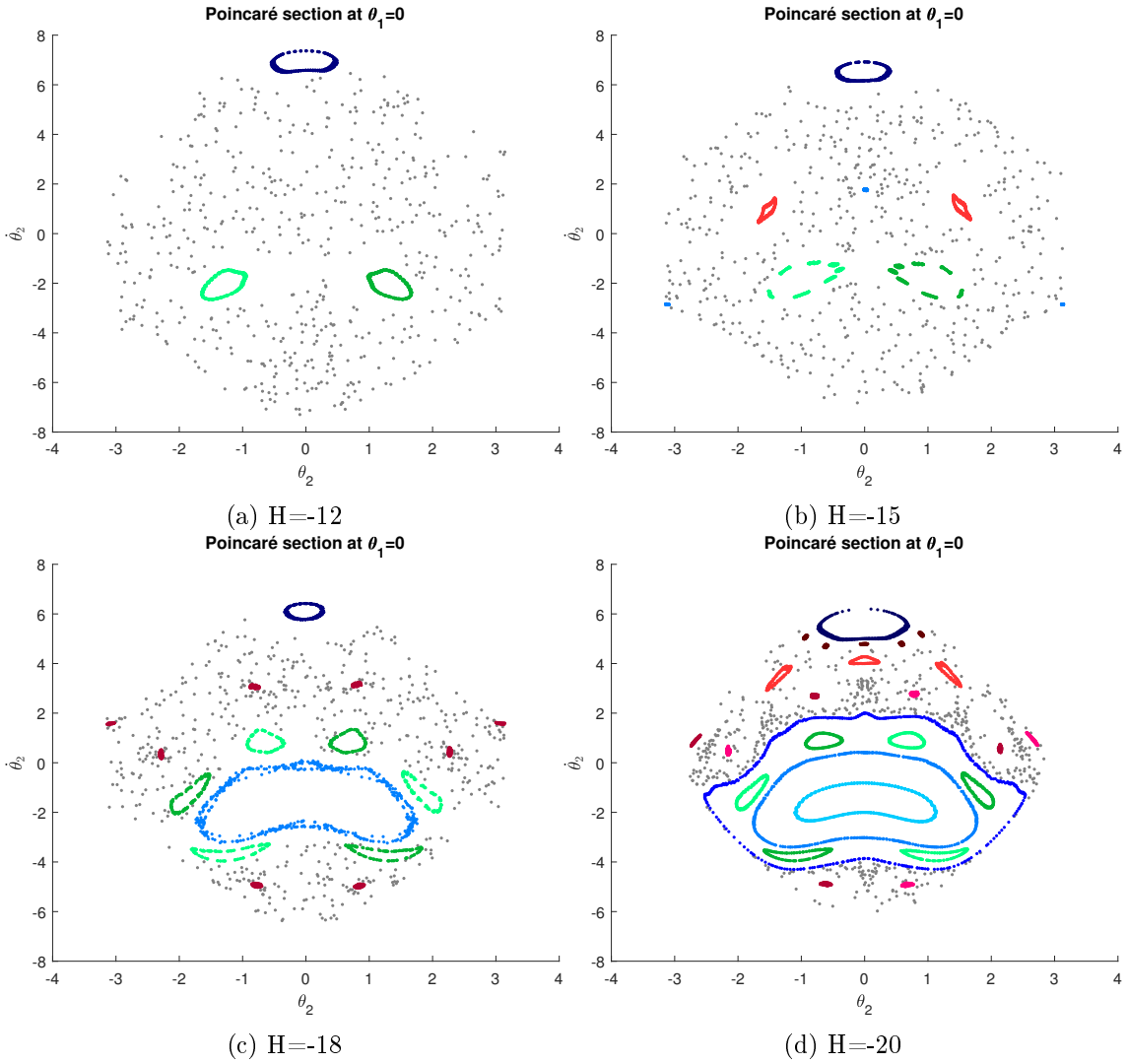

(a) H=-12 (b) H=-15

(c) H=-18 (d) H=-20

Figure 4.6: Decreasing H to find more Poincaré sections. For $H = -20$, many more periodic orbits can be seen. Each of the coloured regions indicates a separate initial condition. The left and right boundary at $\theta_2 = \pm\pi$ become smaller as the amount of energy in the system becomes smaller.

Figure 4.7 shows the same Poincaré section at $H = -20$, now using the symplectic Euler method instead of the Störmer-Verlet method. The result is similar, although the points shown due to the chaotic (grey) trajectory is more spread out, and the second blue 'ring' from the middle out shows gaps in comparison to the using the result using the Störmer-Verlet method (figure 4.6d), i.e. the trajectory resembles a quasi-periodic orbit.

In figure 4.7, it is difficult to see any major differences between the two Poincaré sections. Hence a zoomed-in part of the plot is shown in figure 4.8 to highlight some minor differences. This establishes the robustness with which structures in the Poincaré section can be predicted numerically. Even in case orbits depend sensitively on details of the numerical methods used, the global character and the region of phase space occupied by such orbits remains well defined. This contrasts comparison at the finest level of detail in which close correspondence is lost already after a short time integration.

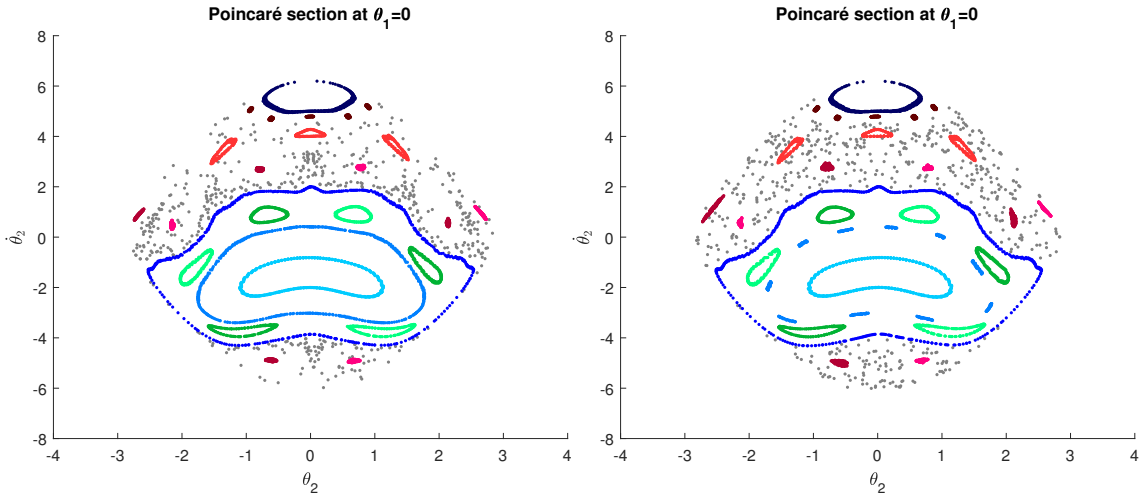

(a) Störmer-Verlet, for reference (b) Symplectic Euler

Figure 4.7: Poincaré section at $H = -20$ using the symplectic Euler method. Each of the coloured regions indicates a separate initial condition. Other than the blue section lying just inside the green periodic orbit, there seems to be no difference.

The time step size Δt is chosen to be equal to 0.01 in all results shown in this chapter in line with section 4.2.2, as we discovered that for this value the results were most interesting, and is in line with the results shown in the next section.

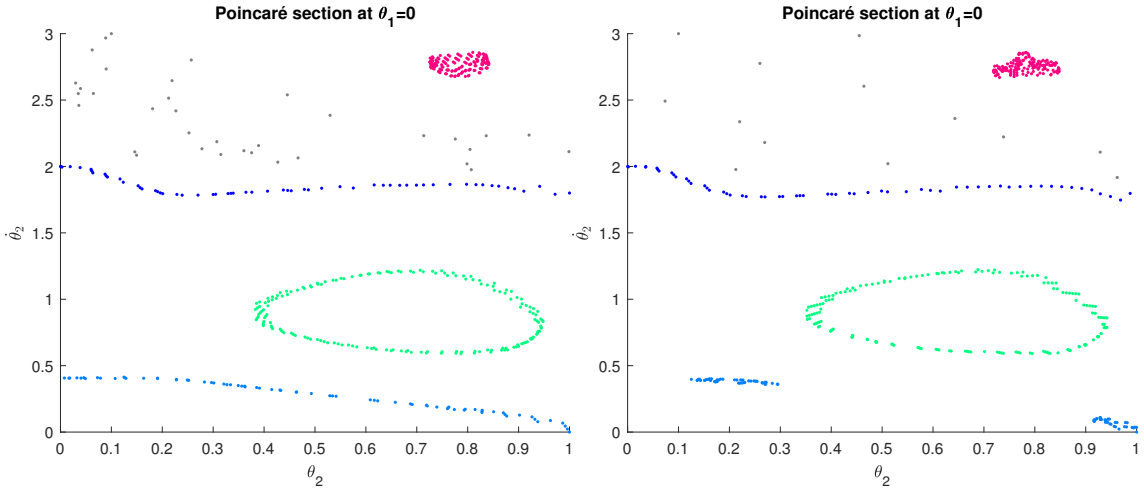

(a) Störmer-Verlet (b) Symplectic Euler

Figure 4.8: Poincaré section at $H = -20$, enlarged. Additional minor differences can be found when zoomed in, such as less chaotic (grey) points being present in the symplectic Euler result, or the pink period showing a different shape.

4.5 Stochastic Poincaré section

In this section, we show and discuss the results of both the stochastic Störmer-Verlet method and the stochastic symplectic Euler method. Both methods are applied to the double pendulum system with Stratonovich multiplicative noise as explained in section 4.3. Recall that these are given by

$$\begin{aligned}
\dot{\theta}_1 &= \frac{\partial H}{\partial p_{\theta_1}} = \frac{l_2 p_{\theta_1} - l_1 p_{\theta_2} \cos(\theta_1 - \theta_2)}{l_1^2 l_2 \left[m_1 + m_2 \sin^2(\theta_1 - \theta_2)\right]} \\
\dot{\theta}_2 &= \frac{\partial H}{\partial p_{\theta_2}} = \frac{l_1 (m_1 + m_2) p_{\theta_2} - l_2 m_2 p_{\theta_1} \cos(\theta_1 - \theta_2)}{l_1 l_2^2 m_2 \left[m_1 + m_2 \sin^2(\theta_1 - \theta_2)\right]} \\
\dot{p}_{\theta_1} &= -\frac{\partial H}{\partial \theta_1} - \beta\theta_1 \circ \mathrm{d}W_t = -(m_1 + m_2) g l_1 \sin\theta_1 - K_1 + K_2 - \beta\theta_1 \circ \mathrm{d}W_t \\
\dot{p}_{\theta_2} &= -\frac{\partial H}{\partial \theta_2} - \beta\theta_2 \circ \mathrm{d}W_t = -m_2 g l_2 \sin\theta_2 + K_1 - K_2 - \beta\theta_2 \circ \mathrm{d}W_t,
\end{aligned} \tag{4.13}$$

where K_1 and K_2 are given in equation (4.3). Parameters and time step values are chosen as discussed in section 4.2.2.

It should be noted that Poincaré sections are used as a tool for systems with constant energy. The addition of noise can cause the total energy to vary. However, the noise is chosen such that the mathematical structure is mostly preserved for a very long time for small values of β, i.e., it can be observed that the total energy over time is almost constant, and at small β do not show an increasing or decreasing trend. Hence, the dynamics can be interpreted as being close to a hyper-surface of constant total energy for all time. This heuristically motivates the use of Poincaré sections also for system that are energy preserving on average only.

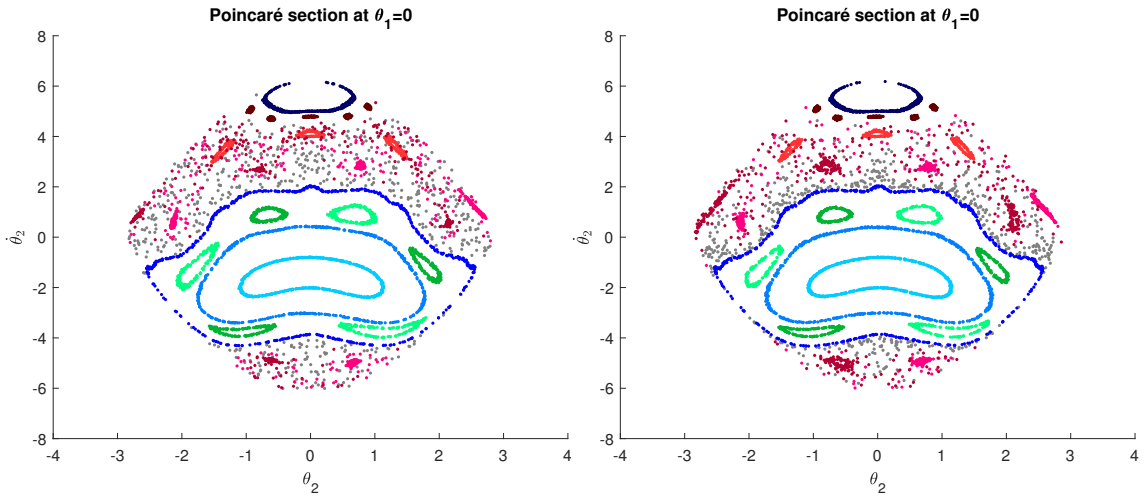

(a) Stochastic Störmer-Verlet (b) Stochastic symplectic Euler

Figure 4.9: Poincaré section at $\theta_1 = 0$ with positive velocity $\dot{\theta}_1$. Here $\beta = 0.001$.

In these simulations, three different values of β are used, namely $\beta = 0.001$ (low amount of noise), $\beta = 0.005$ (medium amount of noise) and $\beta = 0.02$ (high amount of noise). These three values are chosen as this range nicely shows the influence of the noise on the system. The results can be seen in figures 4.9, 4.10 and 4.11 respectively.

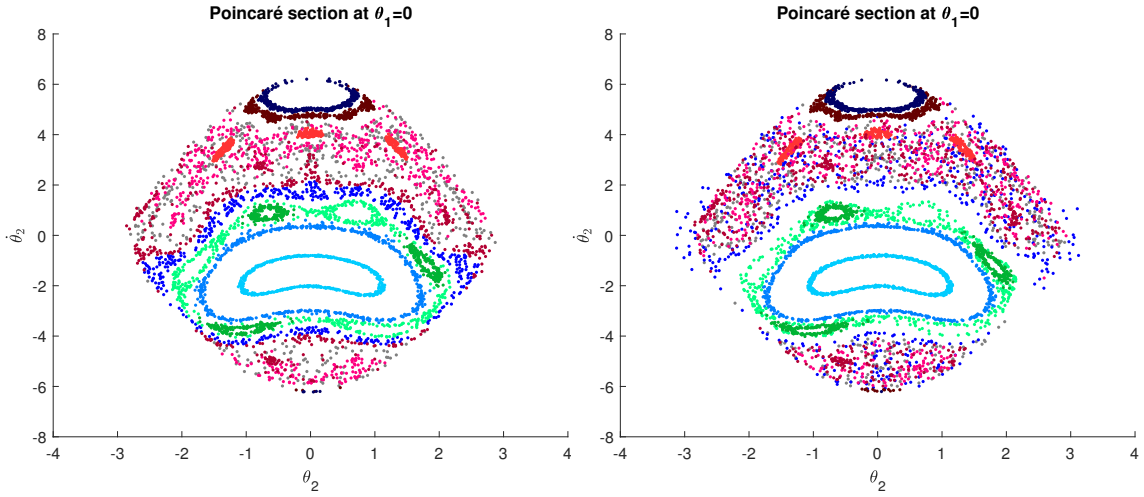

(a) Stochastic Störmer-Verlet (b) Stochastic symplectic Euler

Figure 4.10: Poincaré section at $\theta_1 = 0$ with positive velocity $\dot{\theta}_1$. Here $\beta = 0.005$.

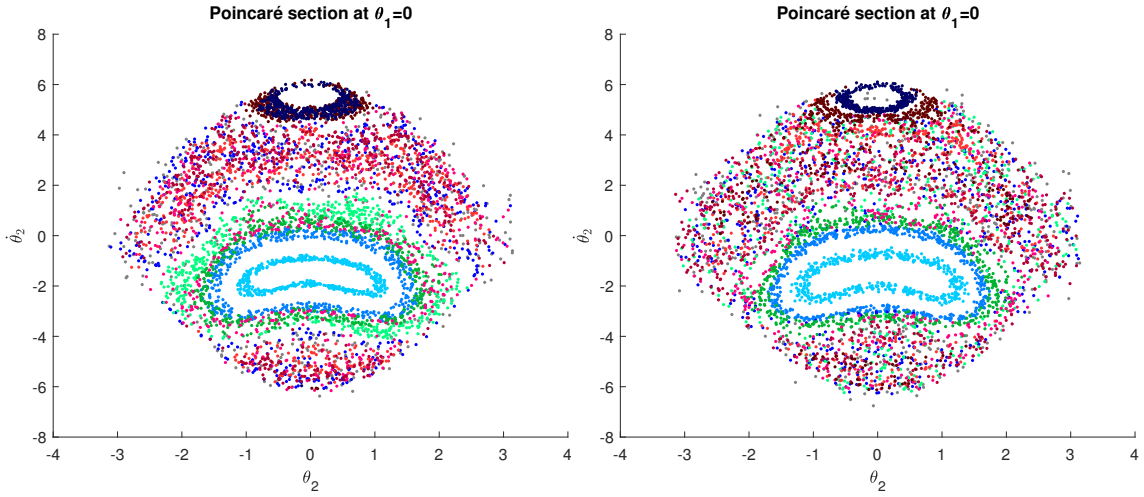

(a) Stochastic Störmer-Verlet (b) Stochastic symplectic Euler

Figure 4.11: Poincaré section at $\theta_1 = 0$ with positive velocity $\dot{\theta}_1$. Here $\beta = 0.02$.

As can be seen in the Poincaré sections, the periodic orbits that were found seem to dissolve as the amount of noise increases. Especially for $\beta = 0.02$, it is hard to recognise any, other than the blue orbits in the middle and the dark blue one on top. The reason these periodic orbit did not dissolve so quickly is most likely due to the fact that the angles for this orbit are very small, causing the noise to have less of an influence. Looking at figure 4.10, trajectories seem to keep their structure more for the Störmer-Verlet method than for the symplectic Euler method, in the way that the blue trajectory in the middle diverges less, and both green trajectories seem to stay in place as well. In figure 4.12, θ_2 of the light blue trajectory as shown in figure 4.11 is observed over time to see if the influence of the noise with $\beta = 0.02$ can be noticed. Checking this for θ_1, we get a similar result. As it is difficult to see any difference in results from this figure, we decide to observe the Fourier transform of θ_2 as well. This is given in figure 4.13.

If we increase the value of Δt slightly such that the deterministic variants of the numerical

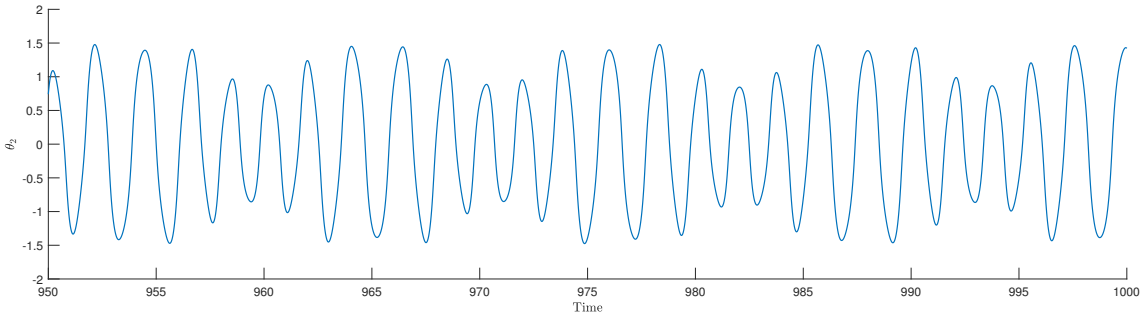

(a) Störmer-Verlet with $\beta = 0$, for reference

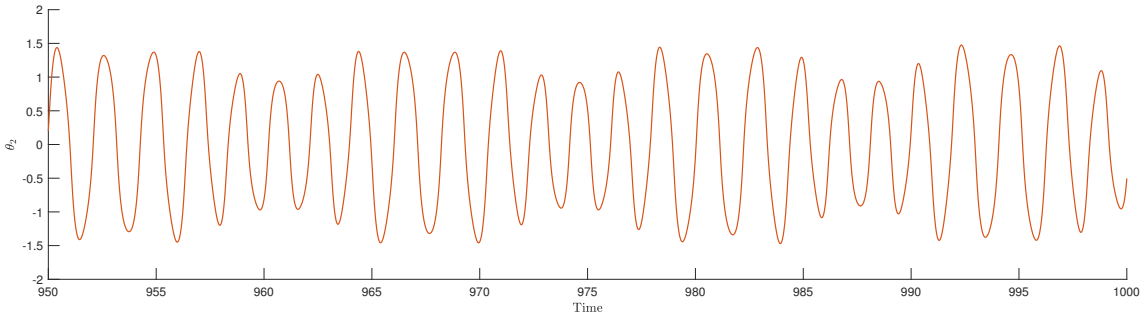

(b) Stochastic Störmer-Verlet

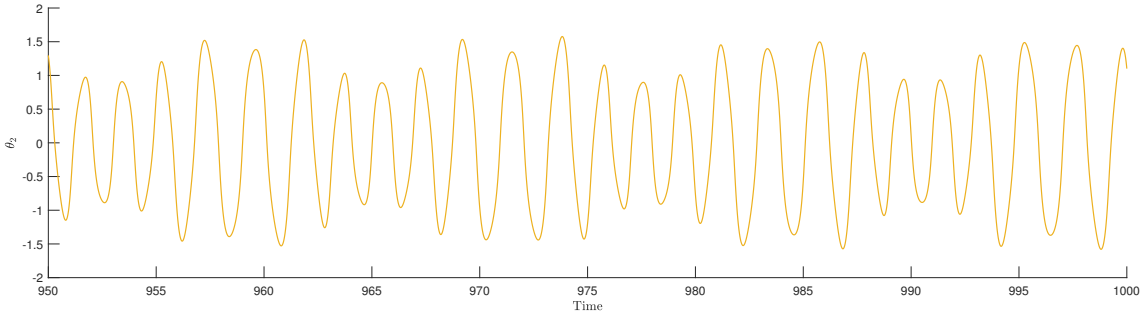

(c) Stochastic symplectic Euler

Figure 4.12: Trajectory of θ_2 over time, for $\beta = 0.02$, corresponding to an initial condition inside the light blue trajectory as shown in figure 4.11. The interval of time was chosen such that a clear difference could be seen, although it can be observed that the amplitudes are not significantly different. A shift in period did happen.

methods keep stable, i.e. $\Delta t < 0.05$, we notice that results do not change significantly, as for smaller values of β the stochastic symplectic Euler solution blows up, while the stochastic Störmer-Verlet method keeps the solution limited, preventing a blow-up.

Zooming in on the images in a similar fashion to figure 4.8, it was found that the images were difficult to interpret and hence did not add value to finding significant differences. For this reason the figures are not included in this document. Similarly, plotting the trajectory of the double pendulum, as discussed in section 4.2, it was found that the plot does not show useful results after simulating for a long running time.

On the other hand,the evolution of the Hamiltonian over time is worth studying. The value of the Hamiltonian can be seen for the different values of β in figure 4.14. This is the value of the Hamiltonian corresponding to a single trajectory. The first thing that stands out is the width of the stochastic symplectic Euler line. The line is much thicker compared

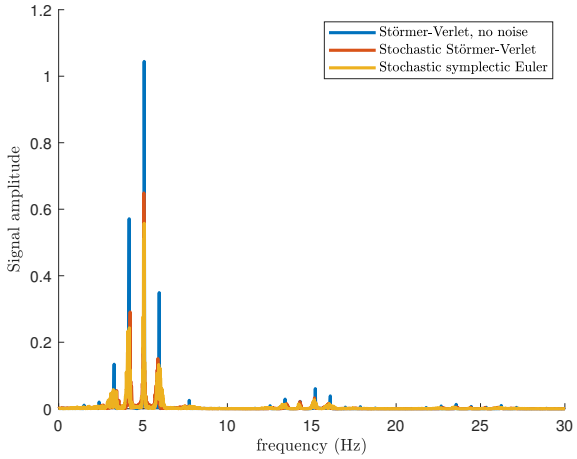

(a) Single-sided amplitude spectrum of θ_2

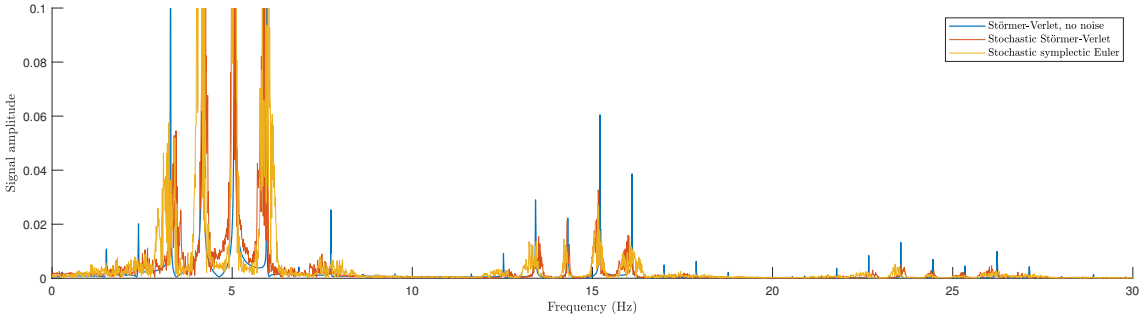

(b) Close-up of the single-sided amplitude spectrum of θ_2

Figure 4.13: Fourier transform of θ_2 over time, for $\beta = 0.02$, corresponding to an initial condition inside the light blue trajectory as shown in figure 4.11. Observe that the amplitude of the peaks for both methods with noise are lower, although the peaks for the stochastic Störmer-Verlet seem a little higher. If we zoom in at the bottom, it can be observed that the symplectic Euler method suffers more from the noise.

to the stochastic Störmer-Verlet method. This is in line with the result from the deterministic method, which shows that the value of the symplectic Euler line fluctuates more, as investigated in figure 4.4. Furthermore, figure 4.14 shows that the noise has a larger impact on the symplectic Euler method. It looks as if the Hamiltonian of the symplectic Euler keeps increasing for $\beta = 0.02$. We have checked whether this is true by plotting it for a much longer period of time and found that the Hamiltonian rapidly increases until it reaches a value where the system breaks, i.e., becomes numerically unstable.

Furthermore, we also look at the value of the Hamiltonian over time for the light blue trajectory, in figure 4.15. It can be seen that the increase in energy over time is less, which makes sense as the structure is preserved even for the high amount of energy.

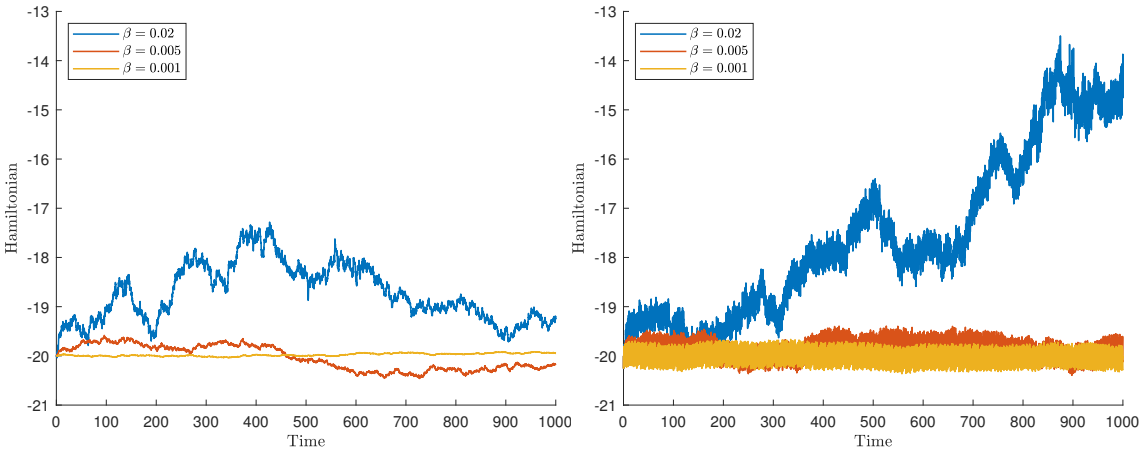

(a) Stochastic Störmer-Verlet (b) Stochastic symplectic Euler

Figure 4.14: Hamiltonians over time for $\beta = 0.02$, $\beta = 0.005$ and $\beta = 0.001$. The value corresponds to the energy level of a single trajectory, namely the grey one (see e.g. figure 4.7), a random example.

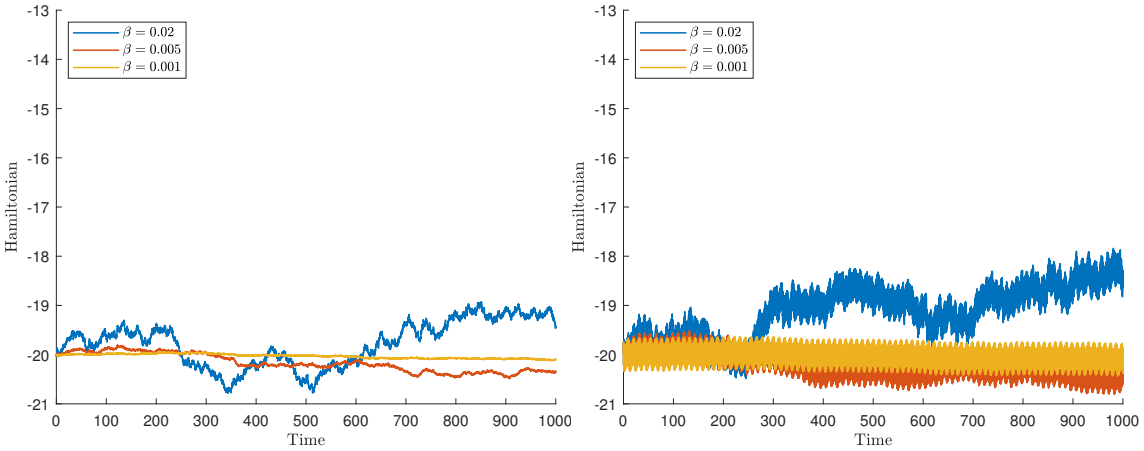

(a) Stochastic Störmer-Verlet (b) Stochastic symplectic Euler

Figure 4.15: Hamiltonians over time for $\beta = 0.02$, $\beta = 0.005$ and $\beta = 0.001$. The value corresponds to the energy level of a single trajectory, namely the light blue one (see e.g. figure 4.7), which we are interested in as the structure is mostly preserved.

4.6 Summary

In this chapter, we looked at the difference of the results of the stochastic Störmer-Verlet method and the stochastic symplectic Euler method for several amplitudes of multiplicative Stratonovich noise. These two methods were chosen since the Euler forward method shows numerical instability and the fourth order Runge-Kutta method shows similar results to the Störmer-Verlet method. The Poincaré section at $\theta_1 = 0$ with positive velocity $\dot{\theta}_1$ was used to determine structures in the double pendulum and to show the difference in simulation between the stochastic Störmer-Verlet method and the stochastic symplectic Euler method.

It was found that the amplification factor β strongly influences the Poincaré section already for small values. Furthermore the differences between the stochastic Störmer-Verlet method and the stochastic symplectic Euler method can be seen in the Poincaré section as well as the value of the Hamiltonian over time. The Störmer-Verlet method does a better job as an integration method. This follows from the boundary of the Poincaré section is more intact, as well as the value of the Hamiltonian is less affected over time.

On the other hand, the value of the Hamiltonian is not precisely constant. The question arises whether there is a way to add noise such that the Hamiltonian does stay intact over time. [10] introduces a stochastic variational principle for fluid dynamics, which does manage to preserve some measured quantities. In a similar way it might be possible to preserve the energy for the double pendulum.

The value of the time step size Δt was chosen such that the simulation had little computational cost and results were of sufficiently high quality. However, as the value of Δt also has a direct relation towards the variance of the Brownian motion, it may be interesting to investigate different values of Δt in further research. An example of an adjusted time step size for $\beta = 0.001$ was considered but no figures were included. Nonetheless, it would be interesting to explore the sensitivity of the solution to adjustments of the time step size.

Chapter 5

Stochastic Lagrangian Drifter

In this chapter we study the Lagrangian drifter. Section 5.1 introduces the Lagrangian drifter and describes the coupling of this model with the physical shallow water model. Section 5.2 describes the basic model of a Lagrangian drifter, both the deterministic as well as the stochastic ones. After establishing these equations, we describe the tools to measure the quality of time integration schemes in section 5.3 using estimates of both the mean as well as the variance of the set of data. In section 5.4 and 5.5 we apply the schemes to explicitly defined velocity fields for which the analytic results are known. Section 5.6 applies the schemes and tests these results for a scenario defined by the shallow water equations.

5.1 Introduction to the Lagrangian drifter

In the previous chapter we considered a model driven by stochastic ordinary differential equations. Now we want to apply the gained knowledge to the study of particle dispersion in a flow. For that we consider the shallow water model, which applies well to many environmental flow problems, e.g., mixing in the upper ocean or in large lakes. The one-dimensional shallow water equations are given by the following set of partial differential equations:

$$\begin{aligned} u_t + \frac{1}{2}(uu)_x + \frac{1}{\mathrm{Fr}^2}(\eta - b)_x &= a(t) \\ \eta_t + (u\eta)_x &= 0. \end{aligned} \tag{5.1}$$

Here, $u(x,t)$ is the velocity field, $\eta(x,t)$ denotes the water height, $b(x)$ denotes the bottom profile underneath the water and $a(t)$ denotes a forcing acting on the water, like the tides. Furthermore, Fr denotes the dimensionless Froude number. An example of a solution $u(x,t)$ at a certain point in time is shown in figure 5.2.

An acclaimed method to make this PDE stochastic is using a stochastically constrained variational principle, as proposed in [10]. The use of this stochastically contrained variational principle causes several quantities to be preserved under the addition of stochasticity. Using this approach, it can be found that the overall equations are adjusted to become

$$\begin{aligned} u_t + \frac{1}{2}(u\hat{u})_x + \frac{1}{\mathrm{Fr}^2}(\eta - b)_x &= a(t) \\ \eta_t + (\hat{u}\eta)_x &= 0. \end{aligned} \tag{5.2}$$

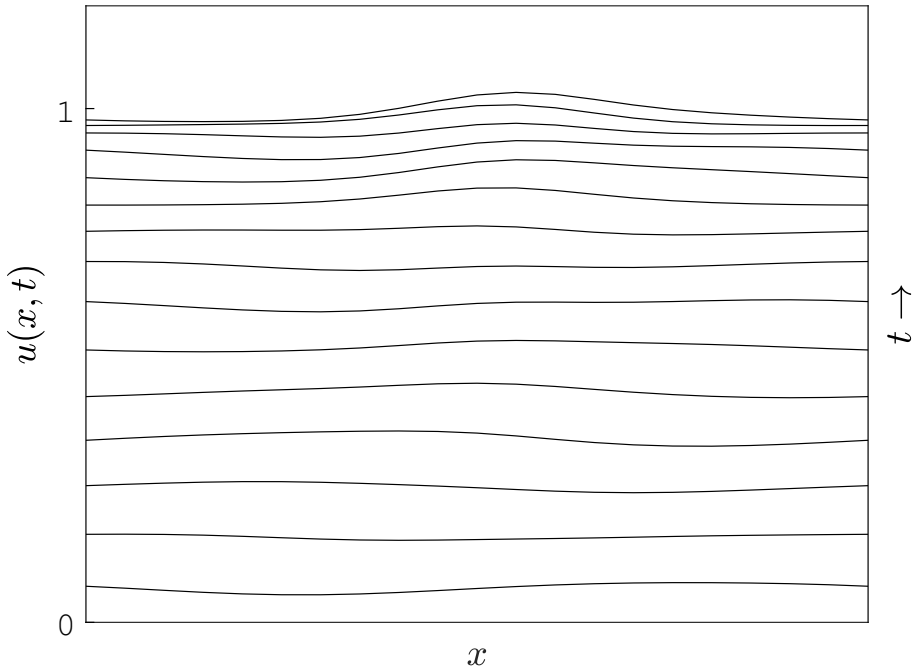

Figure 5.1: Evolution of velocity field $u(x,t)$ over time, with initial conditions $u(x,0) = 0$, $\eta(x,0) = b(x) = 1 - c \cdot \exp\left(\frac{-(x-x_0)^2}{k^2}\right)$, $a(t) = \cos(t)$. Boundary conditions are periodic, i.e. $u(0,t) = u(1,t)$, $\eta(0,t) = \eta(1,t)$. Parameters values are $c = 0.01, k = 0.15, x_0 = 0$ and $\mathrm{Fr} = 0.75$. It can be observed that the motion moves upward until it stops at about $u = 1$, from where the motion will continue in opposite direction. Furthermore, notice that u only changes slightly for different values of x.

Here, $\hat{u}$ is given by

$$\hat{u} = u + \xi_0 + \sum_{i=1}^{m} \xi_i \circ \mathrm{d}W_i, \tag{5.3}$$

where $\xi(x)$ are location-dependent functions that act as amplification factors for the stochastic process. Adding noise in this way preserves several properties, such as potential vorticity (see [32]).

However, due to the nonlinear nature of the shallow water equations, it is hard to verify the preservation of several quantities numerically. Instead, we use the velocity field as described in equation (5.1) and transform it into a Lagrangian function. This means that instead of looking at the flow u over time, we look at individual particles x over time. We call these particles drifters. For example, in the case of ocean dynamics the Lagrangian drifters can be associated with buoys on a large-scale shallow water surface.

5.2 Lagrangian drifter equations

Let us denote the location of drifter d at time t by $x_d(t)$. We assume each drifter has no mass and no friction, meaning the location of each deterministic drifter is directly determined by the flow and does not further affect the evolution of the flow, i.e.,

$$\frac{\mathrm{d}}{\mathrm{d}t} x_d = u(x_d, t). \tag{5.4}$$

Here we have that $x_d(t) \in \mathbb{R}$. This may cause problems, since the velocity field u is only defined on a finite amount of grid points. To tackle this problem, we use linear interpolation to construct a value of $u(x_d, t)$ from the known values of u at the grid points which x_d lies between. Since t is a defined grid on which $u(x_d, t)$ is defined, we do not have to use linear interpolation in this dimension.

Stochastic equations

We now introduce stochastic noise to equation (5.4). The location of the drifter is given, in line with equation (5.3), by

$$\mathrm{d}x_d = u(x_d, t)\mathrm{d}t + \xi_0(x_d, t) + \xi_1(x_d, t) \circ \mathrm{d}W_{d,t}. \tag{5.5}$$

Important is that $W_{d,t}$ is both time as well as drifter dependent. Here, we choose $\xi_1(x_d, t)$ as:

$$\xi_1(x_d, t) = \beta u(x_d, t), \tag{5.6}$$

where β is a constant multiplication factor. The choice of ξ_1 is made with dispersion of large particles in mind. Furthermore, equation (5.6) has a view that if the ocean moves very fast, a ship is more vulnerable to noise.

The ξ_0 term is used to make the analysis simpler. Recall that we can rewrite the Stratonovich differential equation into an Itô differential equation alongside corollary 2.2.1, therefore ξ_0 is chosen such that

$$\mathrm{d}x_d = u(x_d, t)\mathrm{d}t + \beta u(x_d, t)\mathrm{d}W_{d,t}, \tag{5.7}$$

i.e., to compensate for the Stratonovich integral.

Choice of numerical methods

In the following section we will use the methods introduced in chapter 3 that are approximations to equation (3.1), as our problem shown in equation (5.7) is an example of this problem. Hence, the adopted methods are the Euler-Maruyama and the stochastic Runge-Kutta method. Although it was reasoned in chapter 4 that the Euler-Maruyama method was not useful for the model of the double pendulum, we can reconsider it here. The reason for this is that the deterministic variant of the method, i.e. the Euler Forward method, is suitable to estimate a solution of equation (5.4). We do not consider the stochastic symplectic Euler and stochastic Störmer-Verlet method here as they are suitable for problems like equation (3.3), which are not investigated in this chapter.

5.3 Statistical tools

We want to compare time integration methods for the drifter equation and determine to what extent specific methods influence the statistics of the Lagrangian drifters. For any drifter the noise associated with the Brownian motion has the effect that each trajectory is unique. Because of this, we do not analyse the behaviour a single drifter, but rather a group of drifters. The aim is to detect whether increasing the number of observations, i.e., increasing the number of independent drifters, results in the average solution converging towards the solution of the underlying deterministic system given by equation (5.4). Next to that, we introduce the variance of a set of drifters and wish to study whether this

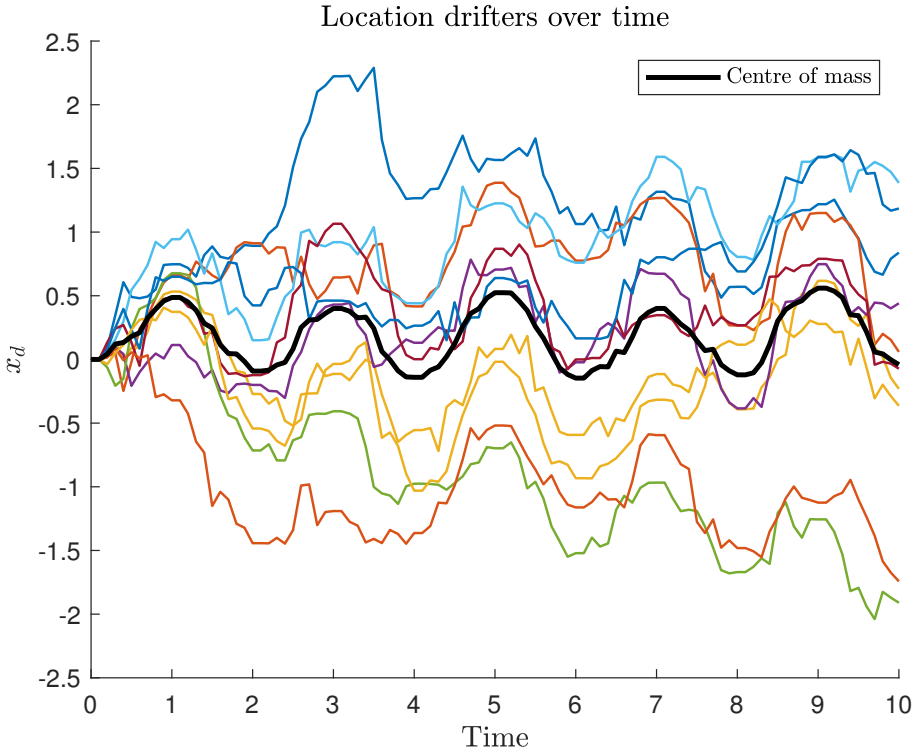

Figure 5.2: Location of 10 drifters over time, driven by a sinusoidal velocity field $u(x,t) = \sin(t)$ and implemented using the Euler-Maruyama method. All drifters start at initial location $x_d(0) = 0$. Notice that the drifters disperse, but do so in a sinusoidal movement. The average location of the drifters, represented by the centre of mass, shows a sinusoidal movement as well.

variance converges towards the analytic value in case an explicitly prescribed velocity field is assumed.

To start our analysis, we will first calculate what the solution should converge to. This amounts to calculating the mean and variance of x_d at a certain chosen time $t = T$. This is done by taking equation (5.7) and calculating the expected value and the variance from the integrated expression, similar to the solution shown in equation (3.2) to the original Itô problem shown in chapter 2 (equation (2.2)). Recall that x_d is the position of drifter d, which moves with both the deterministic and stochastic flow. Thus we find that the value of x_d at time $t = T$ is given by

$$x_d(T) = x_d(0) + \int_0^T u(x_d, t)\mathrm{d}t + \int_0^T \beta u(x_d, t) \circ \mathrm{d}W_{d,t}. \tag{5.8}$$

Here, it is assumed that the initial time t_0 is equal to 0. This assumption is implied for the rest of this chapter. From this expression, we can directly calculate the expected value

and the variance of the solution $x_d(T)$. The expected value is given by

$$\begin{aligned}
\mathrm{E}(x_d(T)) &= \mathrm{E}(x_d(0)) + \mathrm{E}\left(\int_0^T u(x_d,t)\mathrm{d}t\right) + \mathrm{E}\left(\int_0^T \beta u(x_d,t)\mathrm{d}W_{d,t}\right) \\
&= x_d(0) + \int_0^T u(x_d,t)\mathrm{d}t + \\
&\quad \beta \cdot \mathrm{E}\left[\lim_{N\to\infty}\sum_{k=0}^{N} u(x_d,t_k)(W_{d,t_{k+1}} - W_{d,t_k})\right] \\
&= x_d(0) + \int_0^T u(x_d,t)\mathrm{d}t + \\
&\quad \beta \lim_{N\to\infty}\sum_{k=0}^{N} u(x_d,t_k) \cdot \mathrm{E}\left[(W_{d,t_{k+1}} - W_{d,t_k})\right]
\end{aligned} \tag{5.9}$$

From the third property of definition 2.1 it immediately follows that the final term is equal to zero. Here we also used the second property of definition 2.1 to the extent that the noise induced in u by the position of the drifter x_d at time t_k is independent of $W_{t_{k+1}} - W_{t_k}$.

Using the same two properties, i.e., the second and third property of definition 2.1, we can also find the variance of x_d at time $t = T$. This is given by

$$\begin{aligned}
\mathrm{Var}(x_d(T)) &= \mathrm{Var}(x_d(0)) + \mathrm{Var}\left(\int_0^T u(x_d,t)\mathrm{d}t\right) + \mathrm{Var}\left(\int_0^T \beta u(x_d,t)\mathrm{d}W_{d,t}\right) \\
&= \mathrm{Var}\left(\beta \int_0^T u(x_d,t) \circ \mathrm{d}W_{d,t}\right) \\
&= \beta^2 \cdot \mathrm{Var}\left[\lim_{N\to\infty}\sum_{k=0}^{N} u(x_d,t_k)(W_{d,t_{k+1}} - W_{d,t_k})\right] \\
&= \beta^2 \lim_{N\to\infty}\sum_{k=0}^{N} \left(u(x_d,t_k)\right)^2 \cdot \mathrm{Var}\left[(W_{d,t_{k+1}} - W_{d,t_k})\right] \\
&= \beta^2 \lim_{N\to\infty}\sum_{k=0}^{N} \left(u(x_d,t_k)\right)^2 \cdot (t_{k+1} - t_k) \\
&= \beta^2 \int_0^T u(x_d,t)^2\mathrm{d}t
\end{aligned} \tag{5.10}$$

Now that we have an analytic expected value and variance of equation (5.7), we want to calculate these values for the Euler-Maruyama and stochastic Runge-Kutta scheme. This is done to ensure whether these schemes converge towards the expected value and variance as the time step size is decreased. If these values are not equal to the analytic values, then the schemes would be inconsistent[33].

Euler-Maruyama

Assuming a uniform time step size Δt, the mean, or expected value, of x_d at time $t = T$ for the Euler-Maruyama method is given by:

$$\begin{aligned} \mathrm{E}(x_d(T)) &= \mathrm{E}\left(x_d(T-\Delta t) + u(x_d,T)\Delta t + \beta u(x_d,T)\Delta W_{d,T}\right) \\ &= \mathrm{E}(x_d(T-\Delta t)) + \mathrm{E}(u(x_d,T) \\ &= \mathrm{E}(x_d(T-\Delta t)) + u(x_d,T)\Delta t \\ &= \dots \\ &= x_d(0) + \Delta t \sum_{t=0}^{T} u(x_d,t). \end{aligned} \tag{5.11}$$

Here we again use that the expected value of the Brownian motion is zero, as mentioned in chapter 2. Similarly, we can also calculate the variance of x_d at time $t = T$. This is given by:

$$\begin{aligned} \mathrm{Var}(x_d(T)) &= \mathrm{Var}\left[x_d(T-\Delta t) + u(x_d,T)\Delta t + \beta u(x_d,T)\Delta W_{d,T}\right] \\ &= \mathrm{Var}(x_d(T-\Delta t)) + \mathrm{Var}\left(\beta u(x_d,T)\Delta W_{d,T}\right) \\ &= \mathrm{Var}(x_d(T-\Delta t)) + \beta^2 u(x_d,T)^2 \cdot \mathrm{Var}(\Delta W_{d,T}) \\ &= \mathrm{Var}(x_d(T-\Delta t)) + \beta^2 u(x_d,T)^2 \Delta t \\ &= \dots \\ &= \beta^2 \Delta t \sum_{t=0}^{T} u(x_d,t)^2, \end{aligned} \tag{5.12}$$

where it is used that the variance of the Brownian motion $\Delta W_{d,t}$ is equal to Δt. Furthermore we use in the first step that the increments of the Wiener process for each time $\Delta W_{d,t_i}$ are independent, see property two of definition 2.1.

Stochastic Runge-Kutta

Recall that the stochastic Runge-Kutta method is given by

$$x_d(T) = x_d(T-\Delta t) + \frac{1}{6}(k_1 + 2k_2 + 2k_3 + k_4) \tag{5.13}$$

Here we denote $k_1, ..., k_4$ as the internal stages of the Runge-Kutta method, as were introduced for the method in equation (3.6). In this model, these are given by

$$\begin{aligned} k_1 &= u(x_d, T-\Delta t)\Delta t + \beta u(x_d, T-\Delta t)\Delta W_{d,T} \\ k_2 &= u(x_d + k_1/2, T-\Delta t/2)\Delta t + \beta u(x_d + k_1/2, T-\Delta t/2)\Delta W_{d,t} \\ k_3 &= u(x_d + k_2/2, T-\Delta t/2)\Delta t + \beta u(x_d + k_2/2, T-\Delta t/2)\Delta W_{d,t} \\ k_4 &= u(x_d + k_3, T)\Delta t + \beta u(x_d + k_3, T)\Delta W_{d,t}. \end{aligned} \tag{5.14}$$

The mean of the Runge-Kutta method is now given by

$$\begin{aligned} \mathrm{E}(x_d(T)) &= \mathrm{E}\left[x_d(T-\Delta t) + \frac{1}{6}(k_1 + 2k_2 + 2k_3 + k_4)\right] \\ &= \mathrm{E}(x_d(T-\Delta t)) + \frac{1}{6}\left[\mathrm{E}(k_1) + 2\mathrm{E}(k_2) + 2\mathrm{E}(k_3) + \mathrm{E}(k_4)\right] \\ &= \mathrm{E}(x_d(T-\Delta t)) + \frac{\Delta t}{6}\left[u(x_d, T-\Delta t) + 2u(x_d + k_1/2, T-\Delta t/2) + \right. \\ &\qquad \left. 2u(x_d + k_2/2, T-\Delta t/2) + u(x_d + k_3, T)\right]. \end{aligned} \tag{5.15}$$

We remind the reader that linear interpolation is used to determine the velocity field u at each internal location.

Notice that if the velocity field u is independent of the drifter location as well as the time, we obtain

$$\mathrm{E}(x_d(T)) = \mathrm{E}(x_d(T-\Delta t)) + \Delta t \cdot u(x_d, T), \tag{5.16}$$

just as we would have with the Euler-Maruyama scheme, equation (5.11).

Similarly, the equation for the variance is given by:

$$\mathrm{Var}(x_d(T)) = \mathrm{Var}(x_d(T-\Delta t)) + \frac{1}{36}\mathrm{Var}\left[k_1 + 2k_2 + 2k_3 + k_4\right]. \tag{5.17}$$

We will analyse two situations, one where the internal stages are independent and one where they are not. This will show only one option is justified, which is demonstrated by assuming a simple velocity field.

The variance term around the internal stages can only be separated if the variance at each internal stage is independent of the other stages. This is the case when the Wiener process $\Delta W_{d,t}$ at each stage is unique, leading towards the expression

$$\begin{aligned}\mathrm{Var}(x_d(T)) &= \mathrm{Var}(x_d(T-\Delta t)) + \frac{1}{36}\left[\mathrm{Var}(k_1) + 4\mathrm{Var}(k_2) + 4\mathrm{Var}(k_3) + \mathrm{Var}(k_4)\right] \\ &= \mathrm{Var}(x_d(T-\Delta t)) + \frac{\beta^2}{36}\left[u(x_d, T-\Delta t)^2 + 4u(x_d + k_1/2, T-\Delta t/2)^2\right. \\ &\quad \left. + 4u(x_d + k_2/2, T-\Delta t/2)^2 + u(x_d + k_3, T)^2\right]\Delta t.\end{aligned} \tag{5.18}$$

Since it is difficult to say what happens if Δt becomes infinitesimal, we will consider a situation where the velocity field u is independent of the position of the drifter as well as the time. We will verify this in our results in section 5.4. If u is independent of the position of the drifter as well as the time, we have that

$$\begin{aligned}\mathrm{Var}(x_d(T)) &= \mathrm{Var}(x_d(T-\Delta t)) + \frac{\beta^2}{36}\left[u(x_d, T)^2 + 4u(x_d, T)^2\right. \\ &\quad \left. + 4u(x_d, T)^2 + u(x_d, T)^2\right]\Delta t \\ &= \mathrm{Var}(x_d(T-\Delta t)) + \frac{10}{36}\beta u(x_d, t)^2 \Delta t,\end{aligned} \tag{5.19}$$

which is different than the variance shown in equation (5.12). Instead, we have that the variance of this scheme is equal to

$$\mathrm{Var}(x_d(T)) = \frac{10}{36}\beta^2 \Delta t \sum_{t=0}^{T} u(x_d, t)^2. \tag{5.20}$$

Now letting the size of Δt become infinitesimal, this expression does not converge towards the variance of the analytical solution in equation (5.10).

On the other hand, using the same Gaussian increment at each internal stage in equa-

tion (5.17), we find that

$$\begin{aligned}
\mathrm{Var}(x_d(T)) &= \mathrm{Var}(x_d(T-\Delta t)) + \frac{1}{36}\mathrm{Var}\left[k_1 + 2k_2 + 2k_3 + k_4\right] \\
&= \mathrm{Var}(x_d(T-\Delta t)) + \frac{\beta^2}{36}\mathrm{Var}\left[u(x_d, T-\Delta t)\Delta W_{d,t}\right. \\
&\quad + 2u(x_d + k_1/2, T - \Delta t/2)\Delta W_{d,t} \\
&\quad + 2u(x_d + k_2/2, T - \Delta t/2)\Delta W_{d,t} \\
&\quad \left. + u(x_d + k_3, T)\Delta W_{d,t}\right] \\
&= \mathrm{Var}(x_d(T-\delta t)) + \frac{\beta^2}{36}\cdot\left[u(x_d, T-\Delta t)\right. \\
&\quad + 2u(x_d + k_1/2, T - \Delta t/2) + 2u(x_d + k_2/2, T - \Delta t/2) \\
&\quad \left. + u(x_d + k_3, T)\right]^2 \Delta t.
\end{aligned} \tag{5.21}$$

Again, we look at the situation where the velocity field u is independent of the position of the drifter as well as the time.

$$\begin{aligned}
\mathrm{Var}(x_d(T)) &= \mathrm{Var}(x_d(T-\Delta t)) + \frac{\beta^2}{36}\left[u(x_d, T) + 2u(x_d, T)\right. \\
&\quad \left. + 2u(x_d, T) + u(x_d, T)\right]^2 \Delta t \\
&= \mathrm{Var}(x_d(T-\Delta t)) + \frac{\beta^2}{36}\left[6u(x_d, T)\right]^2 \Delta t \\
&= \mathrm{Var}(x_d(T-\Delta t)) + \beta^2 u(x_d, T)^2 \Delta t.
\end{aligned} \tag{5.22}$$

In this case, the same variance is found as in equation (5.12). Both values converge towards the variance shown in equation (5.10) as Δt becomes infinitesimal.

We will from now on denote the expected value and variance of x_d at time T as μ_T and σ_T^2 respectively, and use context to make clear whether we are referring to the expected value and variance of the analytical solution, the solution from the Euler-Maruyama scheme, or the solution from the stochastic Runge-Kutta scheme.

Sample mean and sample variance

We now have clear what mean and variance we could expect from each of our chosen schemes. We now introduce the sample mean and sample variance as a way to measure our results. In respect, these are given by

$$\bar{x}_T = \frac{1}{N}\sum_{d=1}^{N} x_d(T), \tag{5.23}$$

$$S_{x_T}^2 = \frac{1}{N-1}\sum_{d=1}^{N}\left(x_d(T) - \bar{x}_T\right)^2. \tag{5.24}$$

In equations (5.23) and (5.24) we let N denote the number of drifters, $d = 1, \ldots N$. Note that the sample mean can also be seen as the average behaviour of our drifters, i.e., the centre of mass. Properties on the sample mean and sample variance can be found in appendix C. From the results in this appendix we conclude that it is expected that the sample mean and variance should converge towards the mean and variance of the respective scheme as the total number of drifters N is increased. In the following sections we will experimentally show whether this is indeed the case.

Mean Squared Displacement

Another way of justifying the numerical schemes is by using the mean squared displacement (MSD), given at time t by

$$\text{MSD} = \frac{1}{N}\sum_{i=1}^{N} |x^{(i)}(t) - x^{(i)}(0)|^2. \tag{5.25}$$

Here, N is the number of particles released at reference locations $x^i(0)$. Note that equation 5.25 resembles equation (5.24). It is known for the mean squared displacement that for a particle solely driven by a Brownian motion, the MSD at time t is equal to

$$\text{MSD} = 2Dt, \tag{5.26}$$

where D is the diffusion coefficient. This diffusion coefficient has a direct relation to the stochastic process, namely that the Brownian motion forcing this particle has a variance of $2Dt$, while maintaining a mean of 0. Hence we could choose a value for the diffusion coefficient D and study whether the average variance of a set of particles converges towards the value of the MSD as the amount of particles increase. On the other hand, since the particles in our system are not only driven by a Brownian motion, but also by a velocity field, this could only be a good verification if we choose a constant velocity field $u(x,t) = 1$. Still, investigating the effect of a numerical method on the value of the diffusion coefficient D can also be achieved by investigating the value of β in equation (5.7) instead.

Furthermore, since the definition of the mean squared displacement is very similar to the definition of the sample variance, the latter is only used from now on. It is then sufficient to verify that the variance agrees with the analytic value at certain times t.

5.4 Constant drift

In this section we will compare the Euler-Maruyama and the stochastic Runge-Kutta method for a constant drift $u(x,t) = 1$.

For this and the following sections, we have chosen to study the situation where $\Delta t = 0.1$. This is of interest to us since the result by the Euler-Maruyama method and the stochastic Runge-Kutta method become similar for Δt small, as shown in the previous section. Furthermore we have chosen $\beta = 1$, and initial condition $x_d(0) = 0$ for all drifters, as this is generally easy to consider.

As was shown in section 5.3, for a value of u that is not dependent on the location of the drifter as well as the time, the Euler-Maruyama and stochastic Runge-Kutta method (with the same noise in each internal stage) are identical. Hence, we obtain the same result here for these methods, as shown in figure 5.3.

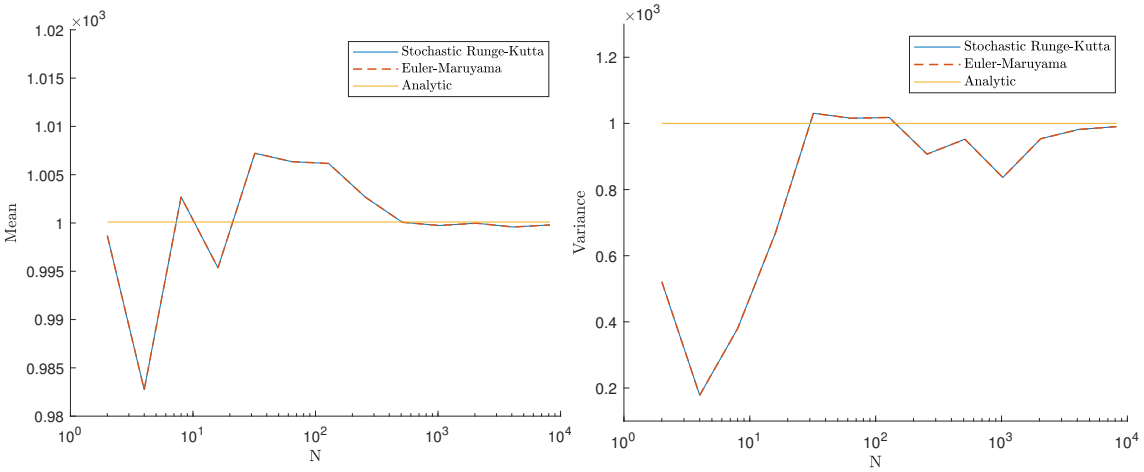

(a) Mean

(b) Variance

Figure 5.3: Mean location and variance of an increasing number of N drifters at $T = 1000$. Both the stochastic Runge-Kutta method and the Euler-Maruyama method converge towards the analytically prescribed mean and variance.

As can be seen in figure 5.3, the mean and variance for both methods converge towards 10^3, which is in line with the theory mentioned in section 5.3.

The mean stays close to the analytical value from $N = 512$ and onward. Repeating this experiment multiple times using new generated Brownian motion, we find that this stays true.

5.5 Sinusoidal drift

In this section we will compare the Euler-Maruyama and the stochastic Runge-Kutta method for a more realistic velocity field, namely a sinusoidal wave $u(x,t) = \sin \pi t$. This velocity field can be thought of as a simple approximation to tidal behaviour. The result of the mean and variance over time can be seen in figure 5.4.

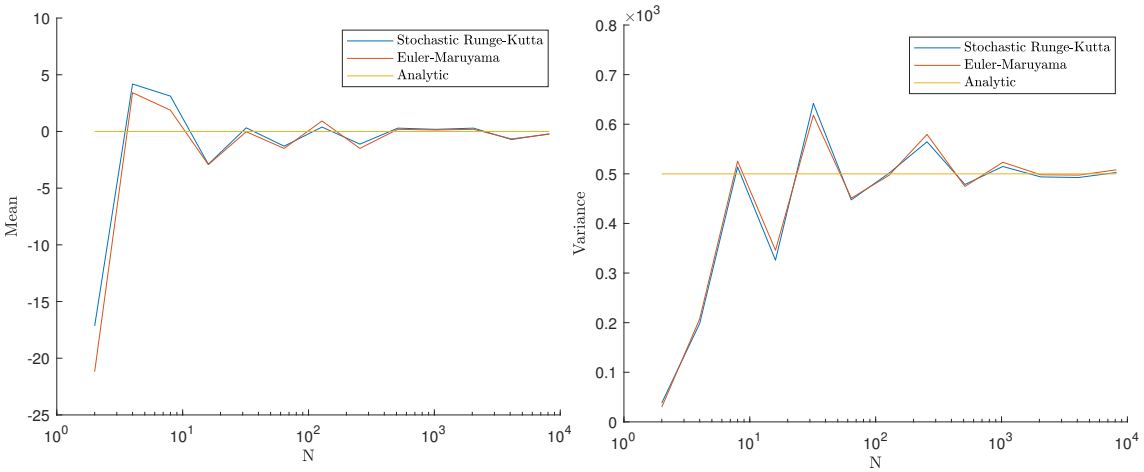

(a) Mean

(b) Variance

Figure 5.4: Mean location and variance of an increasing number of N drifters at $T = 1000$.

As can be observed in figure 5.4, the results of both methods are almost identical. This is likely due to the fact that the time step size is still too small to make a significant impact.

The error between the mean of the numerical methods and the analytic mean seems to be much larger compared to the result generated by the constant drift. If we repeat this experiment with new generated Brownian motion, we find that indeed the error is much larger compared to the error of the constant drift.

Additionally, it can be seen that for less then 10 drifters the error for the expected value seems to be small compared to the error for an increased amount of drifters.

5.6 Drift from a real scenario

In this section, we study the result of both schemes for a velocity field generated by the shallow water equations, as were mentioned in section 4.1. That is, we take u to be the numerically approximated solution of equation (5.1). The results can be seen in figure 5.5.

These figures contain no line showing the true expected value and variance, as the calculation of these values is not available. This is due to the fact that u is dependent on the position of the drifters.

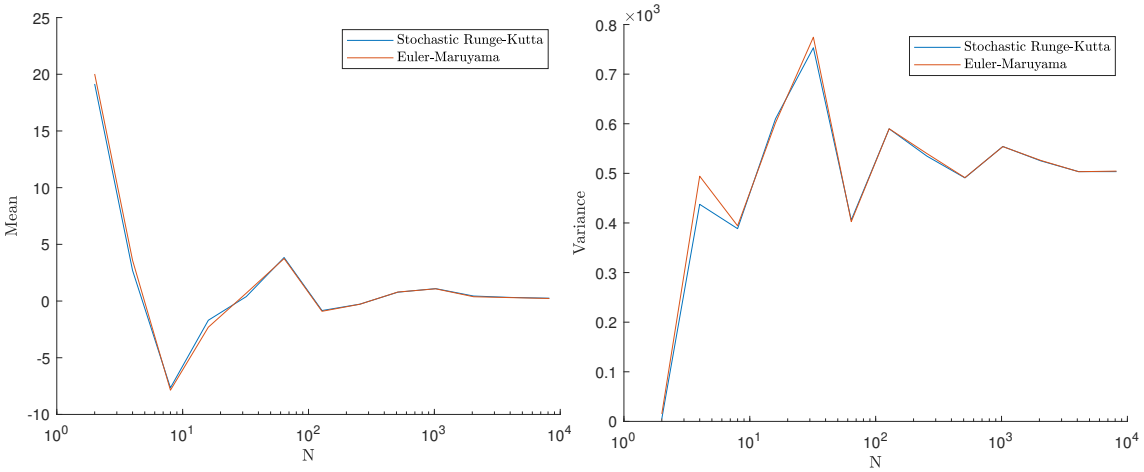

(a) Mean

(b) Variance

Figure 5.5: Mean location and variance of an increasing number of N drifters at $T = 1000$.

In figure 5.5, it can be observed that the two solutions lie very close together. Repeating this experiment with new values for the Brownian motion, we can indeed verify that the solution of the stochastic Runge-Kutta and Euler-Maruyama method are always approximately equal. Initially, it was thought that the difference should be bigger, as the velocity field u is dependent both on the position as well as the time. However, remember the picture shown in figure 5.2. If we look at the solution $u(x,t)$ at any time t generated by equation (5.4), we see that the $u(x,t)$ is is nearly constant in space.

It can also be observed in figure 5.5 that the mean value and variance converge to similar values as for the case of sinusoidal drift. Again this can be confirmed by the behaviour of u from the shallow water equations because u behaves like a sinusoidal over time.

5.7 Summary

In this chapter we studied the difference of the results of the Euler-Maruyama method and the stochastic Runge-Kutta method on the Lagrangian drifter. A noise term was included in the drifter equation by introducing Stratonovich multiplicative noise. Using the variance of the analytic solution, we showed that the Runge-Kutta method could only be justified as an approximation to the solution if the noise in each stage would be the same. Using these methods, we approximated solutions for three different velocity fields $u(x,t)$, namely a constant one, a sinusoidal field, and finally a velocity field generated by the one-dimensional shallow water equations.It was found that the difference between the sample mean and sample variance of the methods were approximately equal, even being exactly equal for the constant velocity field, in line with the theory covered. We conclude that for this problem the Euler-Maruyama method provides a sufficiently accurate approximation to the true solution. Additionally, it is a computationally cheaper method than the stochastic Runge-Kutta method, which uses four internal stages per time step, while the Euler-Maruyama method only uses one.

An additional interesting study presents itself when considering the behaviour of particles on the stochastic shallow water equations using the deterministic variant of the Lagrangian drifter, which can be found in equations (5.2) and (5.4), respectively. These results can subsequently be compared to the location of the particles obtained using the stochastic Lagrangian drifter driven by the deterministic shallow water equations , i.e. the results in section 5.6. This could lead to new insights on how to choose the noise in the stochastic Lagrangian drifter, and forge a relation between equations (5.6) and (5.7).

Chapter 6

Conclusion

In this thesis we have studied the results of two models, which were subjected to a stochastic process. To reach this goal, we have introduced a stochastic variable inside a differential equation in the form of a Wiener process, and shown some basic properties of the stochastic differential equation. This expression has been discretised and numerical methods were introduced to approximate the solution as a function of time.

A model of the double pendulum has been introduced, where we added stochastic terms to the canonical momenta of the Hamiltonian equations. Using Poincaré sections we could analyse the behaviour of the double pendulum under varying levels of multiplicative Stratonovich noise. We focused on two different time integration methods, namely the stochastic Störmer-Verlet method and the stochastic symplectic Euler method, which yielded almost identical results for the deterministic model. For the stochastic model, the results between the two methods were close in terms of preserving the total energy but far from being locally identical for the same noise. For a low level of noise, some structured orbits, e.g., periodic motions, seen in the Poincaré sections, were preserved but most such structured orbits seemed to disappear as a form of chaotic motion. Increasing the amount of energy only amplified this effect, with leaving only basic low frequency orbits seemingly untouched.

We introduced another model of particles floating on top of a field of water. Specifically, we introduced the shallow water equations as an example of an underlying system which moves these particles. Using statistical tools we have shown that the expected value and the variance of the Euler-Maruyama and stochastic Runge Kutta numerical schemes converge towards the expected value and the variance of the continuous model of the stochastic drifter. As expected, for a constant drift the results were equal, and for a sinusoidal drift velocity field the results were still quite close to each other. Even adjusting several parameters did not result in a bigger difference in expected value and variance for the two methods. In the third situation analysed, the drift was induced by the one-dimensional deterministic shallow water equations, as shown in equation (5.1). Similar to the previous two cases, differences in the particle dispersion characteristics were found insensitive to the numerical method, showing that a low order deterministic method would be sufficient.

Appendix A

Extensive proofs SDE's

Lemma A.1

Lemma A.1. *The following equality holds true:*

$$\left[\int_{t_0}^{T} dW_s\right]^2 = \int_{t_0}^{T} ds, \tag{A.1}$$

or, in more detail when written out,

$$(W_{t_{k+1}} - W_{t_k})^2 \to (t_{k+1} - t_k), \text{ whenever } (t_{k+1} - t_k) \to 0, \tag{A.2}$$

for $k \in \{0, 1, 2, ..., N-1\}$.

Proof. Let us denote $\Delta W_{t_k} = W_{t_{k+1}} - W_{t_k}$ and $\Delta t_k = t_{k+1} - t_k$. First of all we show that the lemma is true for the expected value:

$$\begin{aligned} \mathrm{E}[(\Delta W_{t_k})^2] &= \mathrm{Var}(\Delta W_{t_k}) + \mathrm{E}[\Delta W_{t_k}]^2 \\ &= \Delta t_k. \end{aligned} \tag{A.3}$$

Now, when partitions ΔW_{t_k} get infinitesimally small, from the strong law of large numbers we get that

$$P\left(\lim_{N\to\infty} \frac{1}{N} \sum_{k=0}^{N-1} \Delta W_{t_k}^2 = \Delta t_k\right) = 1. \tag{A.4}$$

□

Relation between an Itô and Stratonovich SDE

Theorem A.2. *Let an Itô SDE be given by*

$$dX_t = f(X_t)dt + g(X_t)dW_t, \tag{A.5}$$

where $X_t \in \mathbb{R}^n$ *denotes the state at time* t. *Furthermore assume that* g *is continuously differentiable. Then in integral form, the conversion to a Stratonovich SDE is given by*

$$\int_0^T g(X_t)dW_t = \int_0^T g(X_t) \circ dW_t - \frac{1}{2}\int_0^T \frac{dg}{dx}(X_t)g(X_t)dt \tag{A.6}$$

Proof. This prove makes use of lemma A.1. Let us denote $\Delta W_{t_k} = W_{t_{k+1}} - W_{t_k}$ and $\Delta t_k = t_{k+1} - t_k$.

$$
\begin{aligned}
\int_0^T g(X_t)\mathrm{d}W_t &= \lim_{N\to\infty} \sum_{k=0}^{N-1} g(X_{t_k})(\Delta W_{t_k}) \\
&= \lim_{N\to\infty} \sum_{k=0}^{N-1} \frac{g(X_{t_{k+1}}) + g(X_{t_k})}{2}(\Delta W_{t_k}) - \lim_{N\to\infty} \sum_{k=0}^{N-1} \frac{g(X_{t_{k+1}}) - g(X_{t_k})}{2}(\Delta W_{t_k}) \\
&= \int_0^T g(X_t) \circ \mathrm{d}W_t - \frac{1}{2} \lim_{N\to\infty} \sum_{k=0}^{N-1} \left(g(X_{t_{k+1}}) - g(X_{t_k})\right)(\Delta W_{t_k}) \\
&= \int_0^T g(X_t) \circ \mathrm{d}W_t - \frac{1}{2} \lim_{N\to\infty} \sum_{k=0}^{N-1} \left(\frac{g(X_{t_{k+1}}) - g(X_{t_k})}{X_{t_{k+1}} - X_{t_k}}(X_{t_{k+1}} - X_{t_k})\right)(\Delta W_{t_k}) \\
&= \int_0^T g(X_t) \circ \mathrm{d}W_t - \frac{1}{2} \lim_{N\to\infty} \sum_{k=0}^{N-1} \left(\frac{g(X_{t_{k+1}}) - g(X_{t_k})}{X_{t_{k+1}} - X_{t_k}} \frac{X_{t_{k+1}} - X_{t_k}}{W_{t_{k+1}} - W_{t_k}}\right)(\Delta W_{t_k})^2 \\
&= \int_0^T g(X_t) \circ \mathrm{d}W_t - \frac{1}{2} \lim_{N\to\infty} \sum_{k=0}^{N-1} \left(\frac{g(X_{t_{k+1}}) - g(X_{t_k})}{X_{t_{k+1}} - X_{t_k}} \frac{X_{t_{k+1}} - X_{t_k}}{W_{t_{k+1}} - W_{t_k}}\right)(\Delta t_k) \\
&= \int_0^T g(X_t) \circ \mathrm{d}W_t - \frac{1}{2} \int_0^T \frac{\mathrm{d}g}{\mathrm{d}x}(X_t) \frac{\mathrm{d}X_t}{\mathrm{d}W_t} \mathrm{d}t \\
&= \int_0^T g(X_t) \circ \mathrm{d}W_t - \frac{1}{2} \int_0^T \frac{\mathrm{d}g}{\mathrm{d}x}(X_t) g(X_t) \mathrm{d}t
\end{aligned}
\tag{A.7}
$$

□

Appendix B

Derivation of the Hamiltonian for the double pendulum

In this section, we derive the Hamiltonian equations for the model of the double pendulum. For that, we first write the system of equations as a Lagrangian system, and derive the equations for the Hamiltonian afterwards.

Let a pendulum be given by a certain mass m_1 attached to a solid object with a rigid massless rod of length l_1, and let this have an angle θ_1, with $\theta_1 = 0$ implying the rod would hang straight down. Now suppose we attach another pendulum with a mass m_2 to the first pendulum with another rigid massless rod of length l_2 with an angle θ_2, where $\theta_2 = 0$ would again imply that the second rod is pointing down from the first pendulum. In Cartesian coordinates, the location of both pendula would then be given by:

$$\begin{aligned} x_1 &= l_1 \sin(\theta_1) \\ y_1 &= -l_1 \cos(\theta_1) \\ x_2 &= l_1 \sin(\theta_1) + l_2 \sin(\theta_2) \\ y_2 &= -l_1 \cos(\theta_1) - l_2 \cos(\theta_2). \end{aligned} \tag{B.1}$$

We want to find equations for velocity of both pendula. This gives

$$\begin{aligned} \dot{x}_1 &= l_1 \cos(\theta_1)\dot{\theta_1} \\ \dot{y}_1 &= l_1 \sin(\theta_1)\dot{\theta_1} \\ \dot{x}_2 &= l_1 \cos(\theta_1)\dot{\theta_1} + l_2 \cos(\theta_2)\dot{\theta_2} \\ \dot{y}_2 &= l_1 \sin(\theta_1)\dot{\theta_1} + l_2 \sin(\theta_2)\dot{\theta_2}. \end{aligned} \tag{B.2}$$

The physical energies playing a role in the double pendulum are the kinetic energy T and the potential energy V. In general, these energies are equal to

$$\begin{aligned} T &= \frac{1}{2}mv^2 \\ V &= mgh, \end{aligned} \tag{B.3}$$

where m denotes a mass, v denotes a velocity, g denotes the gravitational constant and h denotes a height. For the double pendulum, the formula for these energies are the

following:

$$\begin{aligned} T &= \frac{m_1}{2}\left(\dot{x}_1^2 + \dot{y}_1^2\right) + \frac{m_2}{2}\left(\dot{x}_2^2 + \dot{y}_2^2\right), \\ V &= m_1 g y_1 + m_2 g y_2. \end{aligned} \tag{B.4}$$

We now use equation (B.2) to transform the energy denoted in Cartesian coordinates into an energy denoted by polar coordinates. For the kinetic energy T, this results in

$$\begin{aligned} T &= \frac{m_1}{2}\left((l_1\cos(\theta_1)\dot{\theta_1})^2 + (l_1\sin(\theta_1)\dot{\theta_1})^2\right) \\ &\quad + \frac{m_2}{2}\left((l_1\cos(\theta_1)\dot{\theta_1} + l_2\cos(\theta_2)\dot{\theta_2})^2 + (l_1\sin(\theta_1)\dot{\theta_1} + l_2\sin(\theta_2)\dot{\theta_2})^2\right) \\ &= \frac{m_1}{2}\left(l_1^2\dot{\theta}_1^2\right) + \frac{m_2}{2}\left(l_1^2\dot{\theta}_1^2 + l_2^2\dot{\theta}_2^2 + 2l_1l_2\dot{\theta}_1\dot{\theta}_2\cos(\theta_1)\cos(\theta_2) + 2l_1l_2\dot{\theta}_1\dot{\theta}_2\sin(\theta_1)\sin(\theta_2)\right) \\ &= \frac{m_1}{2}\left(l_1^2\dot{\theta}_1^2\right) + \frac{m_2}{2}\left(l_1^2\dot{\theta}_1^2 + l_2^2\dot{\theta}_2^2 + 2l_1l_2\dot{\theta}_1\dot{\theta}_2\cos(\theta_1 - \theta_2)\right). \end{aligned} \tag{B.5}$$

Furthermore, the potential energy V in polar coordinates is equal to

$$V = -m_1 l_1 g\cos(\theta_1) - m_2 l_1 g\cos(\theta_1) - m_2 l_2 g\cos(\theta_2). \tag{B.6}$$

The Lagrangian is defined as the difference between the kinetic and the potential energy, i.e., $L = T - V$. This implies that in our case the Lagrangian L is given by

$$\begin{aligned} L(\theta_1, \theta_2, \dot{\theta}_1, \dot{\theta}_2) = \frac{m_1 + m_2}{2}\left(l_1^2\dot{\theta}_1^2\right) + \frac{m_2}{2}\left(l_2^2\dot{\theta}_2^2\right) + m_2 l_1 l_2\dot{\theta}_1\dot{\theta}_2\cos(\theta_1 - \theta_2)\ldots \\ + (m_1 + m_2)l_1 g\cos(\theta_1) + m_2 l_2 g\cos(\theta_2). \end{aligned} \tag{B.7}$$

Next, we want to denote the Euler-Lagrange equation, which is an important equation for Lagrangian mechanics. This says that for a Lagrangian L, the following equality holds

$$\frac{\partial L(\theta, \dot{\theta})}{\partial \theta} = \frac{\mathrm{d}}{\mathrm{d}t}\frac{\partial L(\theta, \dot{\theta})}{\partial \dot{\theta}}. \tag{B.8}$$

For now we will not use this equality explicitly, although we will need it in section 4.3.

$$\begin{aligned} \frac{\partial L}{\partial \dot{\theta_1}} &= (m_1 + m_2)l_1^2\dot{\theta}_1 + m_2 l_1 l_2\dot{\theta_2}\cos(\theta_1 - \theta_2) \\ \frac{\partial L}{\partial \dot{\theta_2}} &= m_2 l_2^2\dot{\theta_2} + m_2 l_1 l_2\dot{\theta_1}\cos(\theta_1 - \theta_2). \end{aligned} \tag{B.9}$$

We now have a Lagrangian and its partial derivatives with respect to $\dot{\theta}$. The equalities in equation (B.9), are known as the canonical momenta of the double pendulum. In this case we denote it by p_θ:

$$p_{\theta_i} = \frac{\partial L}{\partial \dot{\theta_i}}, \quad i = 1, 2. \tag{B.10}$$

For any Lagrangian system L, we can denote it as a Hamiltonian system H as a function of θ and p_θ. This can be done as follows

$$H = \sum_{i=1}^{2} \dot{\theta}_i p_{\theta_i} - L. \tag{B.11}$$

The update of p_θ and θ for a Hamiltonian can then be determined via Hamilton's equations, given by

$$\begin{aligned} \frac{\mathrm{d}\theta}{\mathrm{d}t} &= \frac{\partial H}{\partial p_\theta} \\ \frac{\mathrm{d}p_\theta}{\mathrm{d}t} &= -\frac{\partial H}{\partial \theta}. \end{aligned} \tag{B.12}$$

The latter equation in equation (B.12) follows directly from the Euler-Lagrange equation (B.8).

The Hamiltonian can be written as a function of θ and p_θ, leaving $\dot{\theta}$ out of the function. To do so, we rewrite $\dot{\theta}$ in terms of p_θ using equation (B.9). We can rewrite equation (B.9) in the form

$$\begin{pmatrix} p_{\theta_1} \\ p_{\theta_2} \end{pmatrix} = A \begin{pmatrix} \dot{\theta}_1 \\ \dot{\theta}_2 \end{pmatrix}, \quad A = \begin{pmatrix} (m_1+m_2)l_1^2 & m_2 l_1 l_2 \cos(\theta_1-\theta_2) \\ m_2 l_1 l_2 \cos(\theta_1-\theta_2) & m_2 l_2^2 \end{pmatrix}. \tag{B.13}$$

We can find the inverse of A, if this exists. Since the determinant of A is bigger than zero for nonzero values of l_1, l_2, m_1 and m_2, the inverse does indeed exist. Since the calculation of the inverse is a tedious process, it is omitted. It can be found that $\dot{\theta}$ in terms of p_θ is given by

$$\begin{aligned} \dot{\theta}_1 &= \frac{l_2 p_{\theta_1} - l_1 p_{\theta_2} \cos(\theta_1-\theta_2)}{l_1^2 l_2 \left[m_1 + m_2 \sin^2(\theta_1-\theta_2)\right]} \\ \dot{\theta}_2 &= \frac{-m_2 l_2 p_{\theta_1} \cos(\theta_1-\theta_2) + (m_1+m_2) l_1 p_{\theta_2}}{m_2 l_1 l_2^2 \left[m_1 + m_2 \sin^2(\theta_1-\theta_2)\right]}. \end{aligned} \tag{B.14}$$

Hence, after more algebraic work, the equation for the Hamiltonian of the double pendulum can be found:

$$\begin{aligned} H(\theta_1,\theta_2,p_{\theta_1},p_{\theta_2}) = \frac{l_2^2 m_2 p_{\theta_1}^2 + l_1^2 (m_1+m_2) p_{\theta_2}^2 - 2 m_2 l_1 l_2 p_{\theta_1} p_{\theta_2} \cos(\theta_1-\theta_2)}{2 l_1^2 l_2^2 m_2 \left[m_1 + \sin^2(\theta_1-\theta_2) m_2\right]} \\ -(m_1+m_2) g l_1 \cos(\theta_1) - m_2 g l_2 \cos(\theta_2). \end{aligned} \tag{B.15}$$

Appendix C

Properties of the sample mean and variance

The expected value of the sample mean is

$$\mathrm{E}(\bar{x}_T) = \frac{1}{N}\sum_{d=1}^{N}\mathrm{E}(x_d) = \mu_T. \tag{C.1}$$

Furthermore, the variance is given by

$$\begin{aligned}\mathrm{Var}(\bar{x}_T) &= \mathrm{Var}\left(\frac{1}{N}\sum_{d=1}^{N}x_d\right)\\ &= \frac{1}{N^2}\mathrm{Var}\left(\sum_{d=1}^{N}x_d\right)\\ &= \frac{1}{N^2}\sum_{d=1}^{N}\mathrm{Var}(x_d)\\ &= \frac{\sigma_T^2}{N}.\end{aligned} \tag{C.2}$$

For large N, the variance of the sample mean should thus go to zero.

The expected value of the sample variance is given by

$$\begin{aligned}
\mathrm{E}(S_{x_T}^2) &= \frac{1}{N-1}\sum_{d=1}^{N}\mathrm{E}\left[(x_d-\bar{x}_T)^2\right] \\
&= \frac{1}{N-1}\sum_{d=1}^{N}\mathrm{Var}\left[x_d-\bar{x}_T\right]+\mathrm{E}\left[x_d-\bar{x}_T\right]^2 \\
&= \frac{1}{N-1}\sum_{d=1}^{N}\mathrm{Var}\left[x_d-\frac{1}{N}\sum_{i=1}^{N}x_{i,T}\right]+0 \\
&= \frac{1}{N-1}\sum_{d=1}^{N}\mathrm{Var}\left[\frac{N-1}{N}x_d\right]+\mathrm{Var}\left[\frac{1}{N}\sum_{i\neq d}x_{i,T}\right] \\
&= \frac{1}{N-1}\sum_{d=1}^{N}\frac{(N-1)^2}{N^2}\sigma_T^2+\frac{N-1}{N^2}\sigma_T^2 \\
&= \frac{N-1}{N}\sigma_T^2+\frac{1}{N}\sigma_T^2 \\
&= \sigma_T^2.
\end{aligned} \tag{C.3}$$

The calculation of the variance of the sample variance can be a tedious process. For this reason, we refer the reader to [34] for more detail on the calculation of this, but for now we omit it and note the variance of the sample variance directly. This is given by

$$\mathrm{Var}(S_{x_T}^2) = \frac{\mu_{T4}}{n}-\frac{\sigma^4(n-3)}{n(n-1)}, \tag{C.4}$$

where $\mu_{T4} = E\left[(x_d-\bar{x}_T)^4\right]$ is the fourth central moment of x_T.

Bibliography

[1] K. V. Litvenko and S. M. Prigarin. Numerical stochastic models of sea surface undulation and extreme ocean waves. Numerical Analysis and Applications, 7(4):293–303, 12 2014.

[2] Xuan Xin, Wendi Qin, and Xiaohua Ding. Continuous stage stochastic Runge–Kutta methods. Advances in Difference Equations, 2021(1), 12 2021.

[3] Zhan Tian, Jun Shi, Zhiqiang Gao, and Francesco N. Tubiello. Assessing the impact of future climate change on wheat production in Huang-Huai-Hai Plain in China based on GIS and crop model. In Wei Gao and Hao Wang, editors, Remote Sensing and Modeling of Ecosystems for Sustainability V, volume 7083, page 70830H. SPIE, 8 2008.

[4] M. James Salinger. Climate variability and change: Past, present and future - An overview. In Climatic Change, volume 70, pages 9–29. Springer, 5 2005.

[5] Yukiko Hirabayashi, Masahiro Tanoue, Orie Sasaki, Xudong Zhou, and Dai Yamazaki. Global exposure to flooding from the new CMIP6 climate model projections. Scientific Reports, 11(1), 12 2021.

[6] Kodai Yamamoto, Takahiro Sayama, and Apip. Impact of climate change on flood inundation in a tropical river basin in Indonesia. Progress in Earth and Planetary Science, 8(1), 12 2021.

[7] Sjoukje Y. Philip, Sarah F. Kew, Karin Van Der Wiel, Niko Wanders, Geert Jan Van Oldenborgh, and Sjoukje Y. Philip. Regional differentiation in climate change induced drought trends in the Netherlands. Environmental Research Letters, 15(9):094081, 9 2020.

[8] Don Kulasiri and Wynand Verwoerd. Chapter 1 Modeling solute transport in porous media. In North-Holland Series in Applied Mathematics and Mechanics, volume 44, pages 1–25. Elsevier, 1 2002.

[9] Gisiro Maruyama. Continuous Markov processes and stochastic equations. Rendiconti del Circolo Matematico di Palermo, 4(1):48–90, 1 1955.

[10] Darryl D Holm. Variational Principles for Stochastic Fluid Dynamics. Technical report, 2015.

[11] Bernard J Geurts, Darryl D Holm, and Erwin Luesink. Lyapunov Exponents of Two Stochastic Lorenz 63 Systems. Technical report.

[12] A. Einstein. Über die von der molekularkinetischen Theorie der Wärme geforderte Bewegung von in ruhenden Flüssigkeiten suspendierten Teilchen. Annalen der Physik, 322(8):549–560, 1 1905.

[13] Peter E. Kloeden and Eckhard Platen. Numerical Solution of Stochastic Differential Equations. Springer Berlin Heidelberg, 1992.

[14] Timo Seppäläinen. Basics of Stochastic Analysis.

[15] Andreas Eberle. Introduction to Stochastic Analysis. Technical report, 2019.

[16] Antoine Lejay. An Introduction to Rough Paths. pages 1–59. Springer, Berlin, Heidelberg, 2003.

[17] Darryl D. Holm and Tomasz M. Tyranowski. Stochastic discrete Hamiltonian variational integrators. BIT Numerical Mathematics, 58(4):1009–1048, 12 2018.

[18] Kiyosi Itô. Stochastic integral. Proceedings of the Imperial Academy, 20(8):519–524, 1944.

[19] R. L. Stratonovich. A New Representation for Stochastic Integrals and Equations. SIAM Journal on Control, 4(2):362–371, 5 1966.

[20] Georg A. Gottwald and John Harlim. The role of additive and multiplicative noise in filtering complex dynamical systems. Proceedings of the Royal Society A: Mathematical, Physical and Engineering Sciences, 469(2155), 7 2013.

[21] G. N. Milstein, Yu M. Repin, and M. V. Tretyakov. Symplectic integration of hamiltonian systems with additive noise. SIAM Journal on Numerical Analysis, 39(6):2066–2088, 2002.

[22] P E Kloeden and E Platen. A survey of numerical methods for stochastic differential equations. Technical report, 1989.

[23] K. Burrage and P. M. Burrage. High strong order explicit Runge-Kutta methods for stochastic ordinary differential equations. Applied Numerical Mathematics, 22(1-3 SPEC. ISS.):81–101, 11 1996.

[24] On the nature of vibratory motions II. Blackburn's double pendulum, 1878.

[25] James A. Blackburn, Yang Zhou-jing, S. Vik, H. J.T. Smith, and M. A.H. Nerenberg. Experimental study of chaos in a driven pendulum. Physica D: Nonlinear Phenomena, 26(1-3):385–395, 5 1987.

[26] Mukul K. Gupta, Kamal Bansal, and Arun K. Singh. Mass and length dependent chaotic behavior of a double pendulum. In IFAC Proceedings Volumes (IFAC-PapersOnline), volume 3, pages 297–301. IFAC Secretariat, 2014.

[27] Rajesh Kumar Gupta. Numerical Methods: Fundamentals and Applications. Cambridge University Press, 2019.

[28] Jiri Blazek. Computational fluid dynamics: principles and applications. Butterworth Heinemann, 2015.

[29] Henri Poincaré. Non-Euclidian geometry. Nature, 45:404–407, 1892.

[30] Leo C. Stein. Poincaré section clicker for the double pendulum.

[31] Tomasz Stachowiak and Toshio Okada. A numerical analysis of chaos in the double pendulum. Chaos, Solitons and Fractals, 29(2):417–422, 7 2006.

[32] Darryl D. Holm and Erwin Luesink. Stochastic Wave–Current Interaction in Thermal Shallow Water Dynamics. Journal of Nonlinear Science, 31(2):1–56, 4 2021.

[33] Alfio Quarteroni, Riccardo Sacco, and Fausto Saleri. Numerical Mathematics, Second Edition.

[34] Eungchun Cho and Moon Jung Cho. Variance of Sample Variance. Technical report.